

PCCP

Accepted Manuscript



This is an *Accepted Manuscript*, which has been through the Royal Society of Chemistry peer review process and has been accepted for publication.

Accepted Manuscripts are published online shortly after acceptance, before technical editing, formatting and proof reading. Using this free service, authors can make their results available to the community, in citable form, before we publish the edited article. We will replace this *Accepted Manuscript* with the edited and formatted *Advance Article* as soon as it is available.

You can find more information about *Accepted Manuscripts* in the [Information for Authors](#).

Please note that technical editing may introduce minor changes to the text and/or graphics, which may alter content. The journal's standard [Terms & Conditions](#) and the [Ethical guidelines](#) still apply. In no event shall the Royal Society of Chemistry be held responsible for any errors or omissions in this *Accepted Manuscript* or any consequences arising from the use of any information it contains.

**Electrochemical CO₂ Reduction on Cu₂O-derived Copper Nanoparticles:
Controlling the Catalytic Selectivity of Hydrocarbons**

Recep Kas,¹ Alexander Milbrat,¹ Ruud Kortlever,² Marc T. M. Koper², Guido Mul^{1,*} and Jonas
Baltrusaitis^{1,*}

¹*PhotoCatalytic Synthesis Group, MESA+ Institute for Nanotechnology, Faculty of Science and
Technology, University of Twente, Meander 229, P.O. Box 217, 7500 AE Enschede, The Netherlands*

²*Leiden Institute of Chemistry, Leiden University, Einsteinweg 55, P.O. Box 9502, 2300 RA Leiden, The
Netherlands*

ABSTRACT: The catalytic activity and hydrocarbon selectivity in electrochemical carbon dioxide (CO₂) reduction on cuprous oxide (Cu₂O) derived copper nanoparticles is discussed. Cuprous oxide films with [100], [110] and [111] orientation and variable thickness were electrodeposited by reduction of copper (II) lactate on commercially available copper plates. After initiation of the electrochemical CO₂ reduction by these oxide structures, the selectivity of the process was found to largely depend on the parent Cu₂O film thickness, rather than on the initial crystal orientation. Starting with thin Cu₂O films, besides CO and hydrogen, selective formation of ethylene is observed with very high ethylene-to-methane ratios (~8 to 12). In addition to these products, thicker Cu₂O films yield a remarkably large amount of ethane. Long term Faradaic efficiency analysis of hydrocarbons shows no sign of deactivation of the electrodes after 5 hours of continuous experiment. Online mass spectroscopy studies combined with X-ray diffraction data suggest the reduction of the Cu₂O films in the presence of CO₂, generating a nanoparticulate Cu morphology, prior to the production of hydrogen, CO, and hydrocarbons. Optimizing coverage, number density and size of the copper nanoparticles, as well

as local surface pH, may allow highly selective formation of the industrially important product ethylene.

*corresponding authors: j.baltrusaitis@utwente.nl, g.mul@utwente.nl

INTRODUCTION

Carbon dioxide (CO₂) is the thermodynamically stable product of most hydrocarbon feedstock combustion processes and a significant contributor to the greenhouse effect.¹ The accumulation of CO₂ in the atmosphere has an impact on climate change and could threaten the environment and eventually the worldwide economy.^{2, 3} The conversion of CO₂ into useful products and chemicals is thus a very attractive research area.^{4, 5} A currently proposed approach is the electrocatalytic reduction of CO₂ where the electrons are supplied from renewable energy sources, such as photovoltaics, wind and blue energy.⁶⁻⁸ However, CO₂ reduction into fuels is anticipated to be very challenging, due to the necessary multiple number of proton-coupled electron transfer steps.⁹

Many polycrystalline metals have been analyzed for their activity towards electrocatalytic CO₂ reduction.¹⁰ Among the metal electrodes, copper is the most extensively studied since it is the only metal capable of producing hydrocarbons from CO₂ with reasonable Faradaic efficiencies (FE) in aqueous solutions at ambient conditions of temperature and pressure.^{11, 12} However, high overpotentials required for the activation of CO₂ and rapid degradation of the catalytic activity are the major obstacles for commercializing the process.^{13, 14} Even though the deactivation of the catalytic activity is reported to be suppressed by preparing electrolytes via pre-electrolysis or applying anodic pulses,^{14, 15} the reproducibility and compatibility of these preparation steps are not appropriate for large scale application. The key issue in the current state of electrocatalytic CO₂ reduction is to find a stable and robust cathode material that could selectively convert CO₂ and H₂O to useful products at low overpotentials.¹⁶ Energy efficient processes at low overpotentials were reported using ionic liquids as solvent¹⁷ or pyridine as additive¹⁸. Besides low current densities reported in these studies, the effects of the solvents on the electrolyzer are

unknown. The modification of polycrystalline copper surfaces with different structures might allow for a stable electrode performance in aqueous solutions and energy efficient transformation routes towards energy dense products.¹⁹

Growing oxide films on top of a metallic surface is a widely used method of producing structured electrode surfaces.^{20, 21} Methanol was anticipated to form on cuprous oxide (Cu_2O) coated Cu surfaces.^{22, 23} However, deactivation of these electrodes for methanol production after short reaction times suggests conversion of the oxide films in the process. Recently, thermally produced thick oxide films were reported to decrease the overpotential of product formation without losing activity for extended electrolysis time.^{19, 24-26} The CO_2 electrocatalytic reduction process on these copper oxide films was proposed to take place on *in-situ* produced copper oxide nanoparticles during cathodic reconstruction of the Cu_2O oxide films. The selectivity of the thick films was predominantly towards carbon monoxide (CO) and formic acid at low potentials, contrary to thin oxide films which mainly produced methanol.¹⁹ **Although several aspects of the thermal-oxide derived electrodes have been validated by Kanan and coworkers, the selectivity towards hydrocarbons, and mechanistic pathways explaining formation thereof, have not been extensively described.**

In this study, the performance of electrochemically produced Cu_2O coated copper substrates towards CO_2 reduction is evaluated in terms of selectivity, activity and long term stability. Cu_2O films with surfaces exposing different crystal facets were prepared via controllable, facile, well established electrochemical methods, and the resulting catalytic performance was evaluated using gas chromatography and online electrochemical mass spectroscopy (OLEMS). The effects of the crystal orientation, oxidation state and thickness of the films on the resulting CO_2

electrocatalytic reduction product selectivity will be extensively discussed, with focus on the formation of methane, ethylene and ethane.

EXPERIMENTAL SECTION

Chemicals, materials and Cu₂O film deposition. All working solutions were prepared and all glassware cleaned using deionized water (Millipore MilliQ, 18.2 MΩ cm). Cuprous oxide films were electrodeposited onto copper plates (Alfa Aesar, 99.99 %) from Cu²⁺ containing solutions prepared using 0.4 M CuSO₄ (Sigma Aldrich, ≥99%) and 3 or 4 M lactic acid (Sigma Aldrich) at 60 or 70 °C, according to the procedures described elsewhere.²⁷ The pH of the solution was carefully adjusted between 9 and 12 using solid NaOH (Sigma Aldrich, 98%) and a 1 M NaOH solution. Copper plates were prepared by mechanical polishing using emery paper, followed by cleaning ultrasonically in ethanol and water. The electrodeposition was conducted in a standard three-electrode cell where platinum mesh and Ag/AgCl in 3M NaCl served as counter and reference electrodes, respectively. Galvanostatic deposition was performed at 0.8 and 2 mA/cm² using a potentiostat/galvanostat (PAR, Versastat 3). Specifically, the crystalline morphology was controlled by adapting experimental parameters. Cu₂O films were deposited using a molar lactic acid (LA)/Cu²⁺ ratio of 10 and 7.5 at pH 12 and pH 9, respectively. The deposition times of the films varies depending on the current density applied. Deposition was continued until a total charge of 7 C/cm² was passed through the cell for all samples. Series of [110] oriented films were prepared by passing a variable amount of total electrical charge through the electrochemical cell, ranging from 3 to 11 C/cm² to control the thickness of the film.

The crystalline phase of the films was determined using X-ray diffraction (a Bruker D2 Phaser, equipped with a Cu-K α radiation source operating at 30 kV and 10 mA). Electron microscopy images were taken using a Phillips FEI XL30 FEG-ESEM and FEI Sirion HR-SEM.

Electrochemical CO₂ reduction experiments. Electrochemical CO₂ reduction was carried out in a glass cell using a three electrode assembly at room temperature and pressure. 85 ml of 0.1 M KHCO₃ (Sigma Aldrich, 99.99%) was used as electrolyte at pH 6.8, as obtained after saturation with CO₂ (Linde Gas Benelux 99.99%,). Pt mesh was used as counter electrode and was separated from the working electrode using a proton exchange Nafion 112 membrane (Sigma Aldrich). Ag/AgCl in 3M NaCl was used as a reference electrode and potentials were recalculated with reference to the Reversible Hydrogen Electrode (RHE) scale after the experiments. CO₂ was continuously purged at a rate of 20 ml/min for 30 minutes before each experiment, to attain saturation of the electrolyte. Then the flow rate was decreased to 5 ml/min, during which electrochemical reduction was conducted. The continuously purged headspace of the reactor was approximately 45 ml and the reactor effluent sampled directly via gas chromatography (GC) once every 6 min. The GC was equipped with two different columns (ShinCarbon 2m micropacked column and Rtx-1) for simultaneous separation of CO, CO₂, H₂ and hydrocarbons. A thermal conductivity detector (TCD) and flame ionization detector (FID) were used to perform the quantitative analysis of the gas phase products. The time needed to reach the steady state concentration was approximately 40 minutes (see Figure SI1), so all experiments were conducted for at least 1 hour before gas phase measurement. A control cathodic experiment was conducted at -1.1 V vs RHE by purging N₂ through the reactor since the decomposition of organics associated with the electrodeposition can also yield hydrocarbons.²⁸ No hydrocarbon or CO formation were detected in the absence of CO₂. **Liquid**

products formed during the electrolysis were analyzed off line using High Performance Liquid Chromatography (HPLC) (Prominence HPLC, Shimadzu; Aminex HPX 87-H column, Biorad).

Electrochemical Surface Area Measurements: The relative surface roughness factors of the nanoparticulate surfaces were calculated by measuring their capacitance values in 0.5 M H₂SO₄. Pt mesh was used as a counter electrode and Ag/AgCl was used as reference electrode. After reducing the layers in 0.1 M KHCO₃, cyclic voltammetry (CV) curves were obtained with different scan rates in the potential region where non-faradaic processes occur. The slope of the current density vs scan rate yielded the capacitance value which was normalized to bare copper, to obtain the surface roughness factors ((Figures SI2a and SI2b).

OLEMS measurements: Online electrochemical mass spectroscopy (OLEMS) was used to detect gaseous products formed during CO₂ reduction.^{29, 30} The products were collected with a small hydrophobic tip that was positioned close to the electrode (about 10 μm) with the aid of a camera. The tip was constructed as a porous Teflon cylinder with a diameter of 0.5 mm and an average pore size of 10-14 μm in a Kel-F holder. The tip was connected to the mass spectrometry chamber with a PEEK capillary. Before experiments the tip was cleaned in a solution of 0.2 M K₂Cr₂O₇ in 2 M H₂SO₄ and rinsed thoroughly with Millipore water. A secondary electron multiplier (SEM) voltage of 2,400 V was used for detection of products in a Balzers quadrupole mass spectrometer, except for hydrogen where a SEM voltage of 1,200 V was used. The products were measured while changing the potential of the electrode from 0.0 V to -1.4 V vs. RHE and back at 1 mV s⁻¹.

RESULTS AND DISCUSSION

Electrochemical Deposition of Cu₂O Films. SEM images and the corresponding XRD patterns of as prepared Cu₂O films are shown in Figures 1a-d. The XRD patterns acquired clearly indicate that the crystals obtained are preferentially oriented in either [100], [110] and [111] directions, depending on the applied synthesis conditions. The films grown at pH 12 with a current density of 0.8 mA/cm² exhibit triangular pyramids oriented in the [110] direction where the (100) and (010) facets are exposed.³¹ Increasing the current density to 2 mA/cm² at pH 12 favors the growth in [100] directions with three-faced pyramids, where the sides of the pyramids expose (111) facets.³² At pH 9 the morphology of the crystals evolved to four sided pyramids oriented in the [100] direction exposing (111) facets.²⁷

Electrodeposition of Cu₂O films has been extensively studied and well established from Cu²⁺ solutions in the presence of the surfactants and complexing agents, such as sodium dodecyl sulfate, or lactic acid.³³⁻³⁵ Formation of [111] and [100] oriented films was studied previously extensively,^{32, 36-38} whereas [110] oriented films were reported in a couple of studies and were found to be stable in a very narrow pH range.³¹ Our attempts to reproduce [110] oriented films were successful, but the orientation of the films was found to be different at increasing thickness, which is most likely due to a change in pH and copper concentration during the electrodeposition.³² Nevertheless, we found that increasing the amount of lactic acid at pH 12 yields [110] oriented films with low current densities in a reproducible way.

Electrochemical CO₂ reduction in 0.1 M KHCO₃ on different facets of Cu₂O films. The distribution of the gaseous products obtained during the CO₂ electrochemical reduction at a cathodic potential of -1.1 V vs RHE is presented in Figure 1e. It can be seen that only minor differences exist in the FE of the gaseous products between the different predominant crystal

oriented films. In particular, CO, methane, ethylene and some ethane were gaseous products observed of CO₂ electrochemical reduction. CO desorbs from the surface and is a well-known intermediate for the formation of ethylene and methane.¹⁰ Ethylene was the major product among the hydrocarbons for all of the samples with a small variation in ethylene/methane ratio observed. Ethane formation was detected with low FE for all of the samples investigated. Unfortunately, we were not able to compare the data to the performance of polycrystalline copper electrodes: complete deactivation of polycrystalline copper was observed, before steady state was reached (the reactor was operated as CSTR).

XRD patterns obtained of the samples after the CO₂ experiments were acquired and show that only diffraction lines due to metallic copper are present (See Figure SI3). Thus, in the potential range applied here for CO₂ electrochemical reduction (-0.2V to -1.1 V vs RHE), none of the Cu₂O films were stable, and reduced to metallic copper. The SEM images of the samples shown in Figure 2a-c signify different microscopic morphology of the films obtained after the reduction process, when compared to that before the reduction. When compared to those in Figure 1, the smooth surfaces of the pyramids roughened and the films cracked at the intersection of the pyramids. The higher magnification insets in Figure 2 show that pyramids are now composed of spherical nanometer sized copper domains. As it will be established further using OLEMS studies, CO₂ reduction apparently did not proceed on Cu₂O, but rather on *in situ* formed metallic copper nanoparticles. Even though there is no distinct difference between the samples in terms of their corresponding product selectivity as a function of initial Cu₂O orientation, suggesting the structure of the *in situ* formed copper nanoparticles is not much different, the observed high ethylene selectivity of the electro-catalytically active copper surfaces is distinctly different from the selectivities previously reported for polycrystalline copper, and oxide derived copper

nanoparticles.^{12, 19, 26} Electro-polished polycrystalline copper is well known to produce methane as the major product within the investigated potential range,¹³ while ethane was reported to be a dominant product on copper derived from thermally formed oxide films.¹⁹ Further, in agreement with our product distribution, anodically created oxide films were found to lead to formation of predominantly ethylene, but for these films ethane formation was not observed.²⁶ To further analyze the effect of the structure of the oxide derived copper nanoparticle layer on hydrocarbon selectivity, layers with different thickness were prepared and evaluated in electrocatalytic CO₂ reduction.

Electrochemical CO₂ reduction in 0.1 M KHCO₃ on (110) Cu₂O films of increasing thickness. The XRD patterns of a series of [110] oriented Cu₂O films prepared by passing a different amount of total electrical charge through the electrochemical cell, are shown in Figure 3a. It can be seen that the diffraction line due to the [110] plane becomes more predominant as the thickness of the films increases. Likewise, the intensity of the metallic copper diffraction lines from the substrate decreases, as the thickness of Cu₂O films increases. Growth in the [100] and [111] directions has been reported to be restricted to a localized or spotty deposition, suggesting growth of our films is more homogeneous to explain the observed preferred [110] crystal orientation of our films.³⁷ CO₂ reduction on the thus prepared electrodes was performed in the potential range between -0.2 and -1.1 V vs RHE. A plot of CO and hydrocarbon FE (%) vs. the applied cathodic potential is shown in Figure 3b. For the samples having higher initial oxide thicknesses, CO formation starts at very low overpotentials (~-0.1 V) and reaches a maximum between -0.3 and -0.5 V vs RHE. These observations are consistent with findings on thermally induced oxide derived films of copper.¹⁹ At higher applied potentials, the FE towards CO decreases, and hydrocarbon products start to evolve with onset potentials between -0.65 and

-0.75 V vs RHE. The change in hydrocarbon product distribution (FE (%)) at cathodic potential of -1.1 V vs RHE as a function of thickness is given at Figure 3c. A major observation is that the distribution of the hydrocarbon products changes distinctively from methane to ethane, CO being relatively constant, and ethylene continuously decreasing. No deactivation towards the hydrocarbon production was observed for the thinnest samples over the course of 5 hours (Figure SI4), as compared to polycrystalline copper which was found to rapidly deactivate within 40 minutes.¹⁴

SEM images of the thinnest (3 C/cm²) and the thickest (11 C/cm²) Cu₂O samples after the electrochemical CO₂ reduction process are shown in Figures 4a and b, respectively. The morphology of the thinnest [110] oriented films is not well pronounced, whereas thicker films show characteristic triangular pyramid morphology. It can be seen that the increase in the initial oxide films thickness increases the coverage of the pyramids, which are again composed of the aggregated copper nanoparticles after reduction. As the thickness of the initial oxide films increases, the size of the cracks between the overlapping pyramids decreases and the individual pyramids start to form continuous films. Sample surface roughness, relative to that of bare copper, was measured and is tabulated in Table 1. As the oxide layer thickness increases, the roughness factors of the *in situ* formed nano particulate copper surface increase as well, ranging from 11 for an oxide derived layer produced at 3 C/cm² to 65 for an oxide derived layer produced at 11 C/cm². Additionally, the increase in the geometrical current density as a function of initial oxide layer thickness confirms the increase in surface roughness (Figure SI5).

Even though the FE of the hydrocarbon products clearly decreases for increasing layer thickness (i.e. the selectivity decreases), the overall current density increases (Figure SI5), and hence the decrease in partial current density values (calculated by the product of the overall current density

and the sum of the FE of the gaseous products) is not as significant (Figure 3d). In other words, the production rate of hydrocarbons (and CO₂ conversion rate) only slightly decreases (reflected by the change from 15 to 12 mA/cm²).

Liquid product analysis for the thinnest sample (3 C/cm²), indicated the formation of formic acid as a non-volatile product (Figure SI6). The Faradaic efficiency amounts to approximately 20%. We have not evaluated the formic acid formation for the other samples, and will focus the remainder of the discussion on the changes in volatile hydrocarbon composition.

Extensive research on the relation between the structure of Copper surfaces and the product composition exists. Single crystal copper electrodes by Hori *et al.* showed that stepped surfaces result in higher selectivity towards ethylene.³⁹ Introducing (111) steps on to the (100) basal plane increases the formation of ethylene over methane with the highest ethylene/methane ratio of ~14 observed on Cu(711).⁴⁰ On the other hand, the width of the Cu(100) terraces is suggested to be a decisive factor towards ethylene formation on stepped copper surfaces.⁴¹ Recently Schouten *et al.* proposed that ethylene formation takes place at low overpotentials on Cu(100) through adsorption of CO dimers, whereas at higher potentials both ethylene and methane formation takes place on (100) and (111) facets via a shared intermediate.⁴² Although we appreciate the effect of surface exposed planes on selectivity, we conclude on the basis of the very similar results obtained for the different Cu₂O morphologies that the structure of the Cu nanoparticles *in situ* formed in electrochemical CO₂ reduction are not profoundly different. To explain the dramatic changes in selectivity due to increasing layer thickness thus has to have an alternative origin.

Importantly, the CO dimerization mechanism on Cu(100) is enhanced in alkaline media.⁴³ Therefore, ethylene formation is suggested to take place at conditions of high (local) pH.⁴¹ The trend of product selectivity towards hydrocarbons observed here with increasing oxide layer thickness is then explained by local changes in pH during the electrolysis. Gupta *et al.* modeled the local pH changes during the electrochemical CO₂ reduction in KHCO₃ solutions.⁴⁴ The local pH near the electrode surface during electrolysis is higher than the bulk value and depends on the applied current density, electrolyte concentration, and stirring speed. The increase in surface roughness and the geometrical current density of the Cu films investigated here, likely lead to an increase in local pH due to the observed increase in hydrogen production (Figure SI7) consuming H⁺. The increasing hydrogen FE as a function of film thickness at potentials above -1.0 V vs RHE is in agreement with the increasing current caused by the presence of the higher surface area, providing additional surface sites for hydrogen evolution. The formation of methane and ethylene have been reported to have a distinctly different pH dependence due to the difference in the involvement of protons in their rate limiting step.^{41, 45} As a result, at higher (local) pH, the formation of ethylene from the CO intermediate is preferred over the formation of methane. The increase in the current density of hydrogen evolution reaction and local pH changes could therefore possibly explain the decrease and disappearance of methane with the increasing oxide thickness.

Ethane formation so far has only been observed on very rough surfaces, such as electrodeposited foam-like structures,⁴⁶ as well as thermally produced oxide films reduced by hydrogenation or electrochemically.^{19, 45} Recent calculations on C-C coupling on Cu(211) surfaces suggest the kinetic barriers for the coupling are strongly influenced by the degree of the adsorbed CO hydrogenation.⁴⁷ These kinetic barriers tend to decrease with increasing degree of the surface

bound CO hydrogenation, which can favor ethane. However, the absence of methane formation on the electrodes where ethane is formed suggest the formation is unlikely to occur via the formation of adsorbed $-\text{CH}_3$, which is proposed as an intermediate for methane formation.⁴⁸ The hydrogenation appears to take place after the C-C coupling, such as further reduction of ethylene, in agreement with ethane being formed at the expense of ethylene. Attempts to reduce ethylene on the thickest initial oxide layer electrode directly were unsuccessful due to the broadening and saturation of the ethylene peak in the gas chromatogram, which eventually overlapped with the ethane peak position. However, preliminary OLEMS experiments have demonstrated the hydrogenation of ethylene over Cu surfaces is feasible; results to be published elsewhere.

In order to obtain deeper insight into the role of the cuprous oxide on CO_2 electrochemical reduction, OLEMS studies were conducted on the [111] and [100] oriented films of different thickness. All of the samples prepared by passing 1 to 5 C/cm^2 showed similar catalytic behavior, when analyzed with OLEMS. Therefore, only the 5 C/cm^2 sample is discussed in detail. The CV graphs obtained are shown in Figure 5, together with the corresponding mass spectroscopy data. Specifically, the very first cathodic sweep is shown in Figure 5a, whereas the following, second sweep, is shown in Figure 5b. A clear reductive wave can be observed in Figure 5a, which is absent in Figure 5b. This is due to the decomposition of electrodeposited cuprous oxide, which starts around -0.3 V vs RHE . Since this process always proceeds during the initial cathodic sweep, all electrochemical CO_2 reduction proceeds on the newly *in situ* formed metallic copper particles and not on as-deposited Cu_2O , in agreement with our data presented earlier. The dashed vertical line in Figure 5a corresponds to the potential where a total charge of 5 C/cm^2 was passed through the electrode for the reduction of the films. Importantly, in the first and the consecutive forward scans no mass fragments corresponding to hydrogen and ethylene were

detected, until reaching the conditions needed for the reduction of the films. At the same potentials, appreciable amount of hydrogen and ethylene is produced during the reverse scan, as well as the second and the following sweep cycles.

Copper oxides are known to form spontaneously on copper when exposed to air or electrolyte solution.⁴⁹ Intentionally formed Cu₂O films on copper have been reported to yield methanol with very high FE.^{23, 50} However, the catalytic activity of these degrades quickly, which is attributed to the decomposition of cuprous oxide to copper, and methanol is considered to be only formed during the reduction of these oxide films. Further, the initial composition of the copper oxide electrocatalyst surface and its transformations during the reduction process are not exactly known. Spectroscopic analysis of spent CO₂ electroreduction electrodes indicate the presence of Cu(I) and Cu(II) oxides after the reaction,⁵⁰ but *in situ* analysis is required to verify the existence of the oxide films during the electrocatalytic process. Using OLEMS, no noteworthy amount of methanol was detected from the samples evaluated here. This once again suggests that gaseous CO₂ electrocatalytic reduction products is governed by the copper metal formed from the Cu₂O films during *in situ* transformations.

Conclusions

This research highlights the selectivity in electrocatalytic CO₂ reduction of copper nanoparticles derived from different Cu₂O morphologies and surface coverages. The orientation of electrodeposited Cu₂O ([110], [111] and [100]) has only a minor effect on the product selectivity. The initial oxide thickness, however, strongly influences the selectivity of the electrocatalytic process. Specifically, OLEMS studies show that the Cu₂O reduction itself seems to be highly favored, when compared to CO₂ reduction or water splitting, since no products were detected by

online mass spectroscopy on as deposited Cu₂O. Further, the catalytic behavior is predominantly determined by layer thickness associated local pH changes, impacting the hydrocarbon selectivities. The optimum number density of nanoparticles with the combination of the right electrolyte (pH) can open up routes for highly selective ethylene formation via electrochemical reduction of CO₂ in reactors. In addition, gas diffusion electrodes or high pressure can be used to improve CO₂ mass transport.

Acknowledgements

This work is supported by NanoNextNL, a micro and nanotechnology consortium of the Government of the Netherlands and 130 partners. We would like to thank Dr. Youngkook Kwon from Leiden University for mass spectrometry measurements. We would also like to thank Dr. Engin Karabudak for fruitful discussions.

Notes and references

Electronic Supplementary Information (ESI) available: details on Faradaic efficiency calculations, steady state reactor conditions, XRD of reduced Cu₂O coatings, long term stability analysis at constant potential, FE of H₂ evolution and CV curves of different thickness oxides. See DOI: 10.1039/b000000x/

1. D. M. D'Alessandro, B. Smit and J. R. Long, *Angew. Chem. Int. Ed.*, 2010, **49**, 6058-6082.
2. S. Solomon, D. Qin, M. Manning, Z. Chen, M. Marquis, K. Averyt, M. Tignor and H. Miller, Contribution of Working Group I to the Fourth Assessment Report of the Intergovernmental Panel on Climate Change, Cambridge University Press, UK and New York, NY, USA, 2007.
3. M. M. Halmann and M. Steinberg, *Greenhouse gas carbon dioxide mitigation: science and technology*, CRC press, 1999.
4. S. K. Ritter, *Chem. Eng. News*, 2007, **85**, 11-17.
5. G. A. Olah, G. S. Prakash and A. Goepfert, *J. Am. Chem. Soc.*, 2011, **133**, 12881-12898.
6. R. E. Blankenship, D. M. Tiede, J. Barber, G. W. Brudvig, G. Fleming, M. Ghirardi, M. R. Gunner, W. Junge, D. M. Kramer, A. Melis, T. A. Moore, C. C. Moser, D. G. Nocera, A. J. Nozik, D. R. Ort, W. W. Parson, R. C. Prince and R. T. Sayre, *Science*, 2011, **332**, 805-809.

7. C. Graves, S. D. Ebbesen, M. Mogensen and K. S. Lackner, *Renew Sust. Energy Rev.*, 2011, **15**, 1-23.
8. G. Mul, C. Schacht, W. P. van Swaaij and J. A. Moulijn, *Chem. Eng. Process.*, 2012, **51**, 137-149.
9. B. Kumar, M. Llorente, J. Froehlich, T. Dang, A. Sathrum and C. P. Kubiak, *Annu. Rev. Phys. Chem.*, 2012, **63**, 541-569.
10. Y. Hori, in *Modern aspects of electrochemistry*, Springer, 2008, pp. 89-189.
11. H. Shibata, J. A. Moulijn and G. Mul, *Catal. Lett.*, 2008, **123**, 186-192.
12. Y. Hori, A. Murata, R. Takahashi and S. Suzuki, *J. Am. Chem. Soc.*, 1987, **109**, 5022-5023.
13. M. Gattrell, N. Gupta and A. Co, *J. Electroanal. Chem.*, 2006, **594**, 1-19.
14. Y. Hori, H. Konishi, T. Futamura, A. Murata, O. Koga, H. Sakurai and K. Oguma, *Electrochim. Acta*, 2005, **50**, 5354-5369.
15. R. Shiratsuchi, Y. Aikoh and G. Nogami, *J. Electrochem. Soc.*, 1993, **140**, 3479-3482.
16. D. T. Whipple and P. J. A. Kenis, *J Phys Chem Lett*, 2010, **1**, 3451-3458.
17. B. A. Rosen, A. Salehi-Khojin, M. R. Thorson, W. Zhu, D. T. Whipple, P. J. Kenis and R. I. Masel, *Science*, 2011, **334**, 643-644.
18. G. Seshadri, C. Lin and A. B. Bocarsly, *J. Electroanal. Chem.*, 1994, **372**, 145-150.
19. C. W. Li and M. W. Kanan, *J. Am. Chem. Soc.*, 2012, **134**, 7231-7234.
20. X. Jiang, T. Herricks and Y. Xia, *Nano Lett.*, 2002, **2**, 1333-1338.
21. Y. Chen and M. W. Kanan, *J. Am. Chem. Soc.*, 2012, **134**, 1986-1989.
22. T. Y. Chang, R. M. Liang, P. W. Wu, J. Y. Chen and Y. C. Hsieh, *Mater. Lett.*, 2009, **63**, 1001-1003.
23. M. Le, M. Ren, Z. Zhang, P. T. Sprunger, R. L. Kurtz and J. C. Flake, *J. Electrochem. Soc.*, 2011, **158**, E45-E49.
24. Y. Chen, C. W. Li and M. W. Kanan, *J. Am. Chem. Soc.*, 2012, **134**, 19969-19972.
25. J. Qiao, P. Jiang, J. Liu and J. Zhang, *Electrochem. Commun.*, 2014, **38**, 8-11.
26. W. Tang, A. A. Peterson, A. S. Varela, Z. P. Jovanov, L. Bech, W. J. Durand, S. Dahl, J. K. Nørskov and I. Chorkendorff, *Phys. Chem. Chem. Phys.*, 2012, **14**, 76-81.
27. T. D. Golden, M. G. Shumsky, Y. Zhou, R. A. VanderWerf, R. A. Van Leeuwen and J. A. Switzer, *Chem. Mater.*, 1996, **8**, 2499-2504.
28. C.-C. Yang, Y.-H. Yu, B. van der Linden, J. C. Wu and G. Mul, *J. Am. Chem. Soc.*, 2010, **132**, 8398-8406.
29. R. Kortlever, K. H. Tan, Y. Kwon and M. T. M. Koper, *J. Solid State Electrochem.*, 2013, **17**, 1843-1849.
30. A. H. Wonders, T. H. M. Housmans, V. Rosca and M. T. M. Koper, *J. Appl. Electrochem.*, 2006, **36**, 1215-1221.
31. L. Wang, N. De Tacconi, C. Chenthamarakshan, K. Rajeshwar and M. Tao, *Thin Solid Films*, 2007, **515**, 3090-3095.
32. S. Joseph and P. V. Kamath, *J. Electrochem. Soc.*, 2007, **154**, E102-E106.
33. A. A. V. Julie K. Barton, Eric W. Bohannon, and Jay A. Switzer, *Chem. Mater.*, 2001, **13**, 952-959.
34. S. Joseph and P. V. Kamath, *Solid State. Sci.*, 2008, **10**, 1215-1221.
35. M. J. Siegfried and K. S. Choi, *Adv. Mater.*, 2004, **16**, 1743-1746.
36. M. G. S. Teresa D. Golden, Yanchun Zhou, Rachel A. VanderWerf, Robert A. Van Leeuwen, and Jay A. Switzer, *Chem. Mater.*, 1996, **8**, 2499-2504.
37. A. E. Rakhshani and J. Varghese, *J. Solar Energy Mater*, 1987, **15**, 237-248.
38. W. Septina, S. Ikeda, M. A. Khan, T. Hirai, T. Harada, M. Matsumura and L. M. Peter, *Electrochim. Acta*, 2011, **56**, 4882-4888.
39. Y. Hori, I. Takahashi, O. Koga and N. Hoshi, *J. Phys. Chem. B*, 2001, **106**, 15-17.
40. Y. Hori, H. Wakebe, T. Tsukamoto and O. Koga, *Surf. Sci.*, 1995, **335**, 258-263.
41. K. J. P. Schouten, E. Pérez Gallent and M. T. M. Koper, *ACS Catalysis*, 2013, **3**, 1292-1295.

42. K. J. P. Schouten, Z. Qin, E. P. Gallent and M. T. M. Koper, *J. Am. Chem. Soc.*, 2012, **134**, 9864-9867.
43. F. Calle-Vallejo and M. T. M. Koper, *Angew. Chem. Int. Ed.*, 2013, **52**, 7282-7285.
44. N. Gupta, M. Gattrell and B. MacDougall, *J. Appl. Electrochem.*, 2006, **36**, 161-172.
45. Y. Hori, R. Takahashi, Y. Yoshinami and A. Murata, *J. Phys. Chem. B*, 1997, **101**, 7075-7081.
46. M. R. Gonçalves, A. Gomes, J. Condeço, T. R. C. Fernandes, T. Pardal, C. A. C. Sequeira and J. B. Branco, *Electrochimica Acta*, 2013, **102**, 388-392.
47. J. H. Montoya, A. A. Peterson and J. K. Nørskov, *ChemCatChem*, 2013, **5**, 737-742.
48. K. J. P. Schouten, Y. Kwon, C. J. M. van der Ham, Z. Qin and M. T. M. Koper, *Chemical Science*, 2011, **2**, 1902-1909.
49. M. Pourbaix, *Atlas of electrochemical equilibria in aqueous solutions*, National Association of Corrosion Engineers, 1974.
50. K. W. Frese, *J. Electrochem. Soc.*, 1991, **138**, 3338-3344.

Tables

Table 1. The capacitance values and surface roughness factors of the films as a function of initial thickness of the films.

Charge passed through	Capacitance	Surface Roughness Factor
Bare Copper	0.14 mF	1
3 C/cm ²	1.6 mF	11
5 C/cm ²	2.4 mF	17
7 C/cm ²	5.1 mF	36
9 C/cm ²	6.1 mF	44
11 C/cm ²	9.1 mF	65

Figures

Figure 1. SEM images of as deposited Cu_2O films with predominant a) [110], b) [111] and c) [100] orientations. d) X-ray diffraction patterns of Cu_2O films electrochemically deposited on copper substrate. e) FE of gaseous products from CO_2 reduction at -1.1 V vs RHE in 0.1 M KHCO_3 solution for oxides having different crystal orientation.

Figure 2. SEM images of copper nanoparticles obtained after reaction from oxides in the a) [110], b) [111] and c) [100] orientations. Corresponding SEM images are also shown with high resolution images in the inset.

Figure 3. a) The X-ray diffraction patterns of the [110] oriented Cu_2O films prepared by changing the total charge passed through the cell. b) FEs of CO and hydrocarbons at different potentials as a function of initial thickness of the films c) FE and d) partial current density of gaseous products from CO_2 reduction at -1.1 V vs RHE in 0.1 M KHCO_3 solution as a function of initial thickness of the films (FEs of CO are given in a limited potential range for clarity).

Figure 4. SEM image of the [110] oriented a) thinnest (3 C/cm^2) and the b) thickest (11 C/cm^2) Cu_2O samples after the electrochemical CO_2 reduction.

Figure 5. Ion currents for methane, ethylene, hydrogen probed by OLEMS as a function of applied potential. Cyclic voltammetry curve of oxide films on copper in CO_2 saturated 0.1 M KHCO_3 solution a) first scan b) second scan (scan rate 1 mV s^{-1}). Arrows indicate the forward and backward scans for clarity.

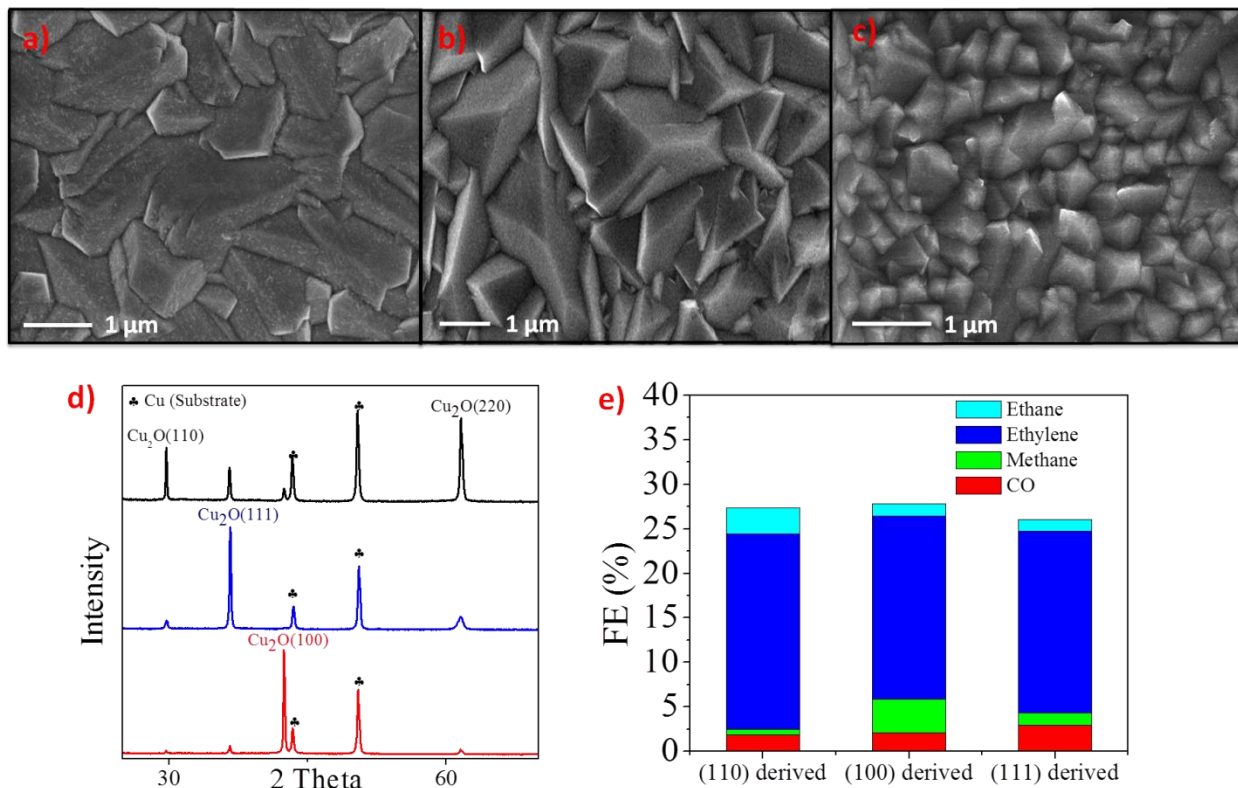


Figure 1

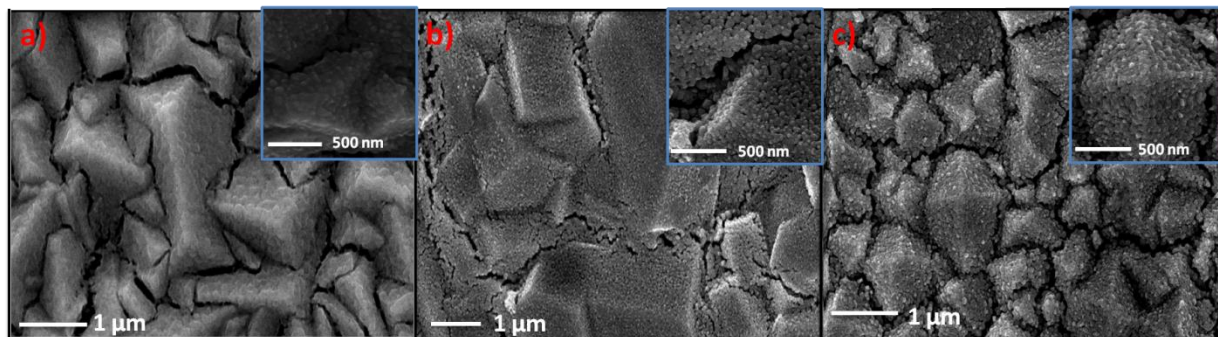


Figure 2

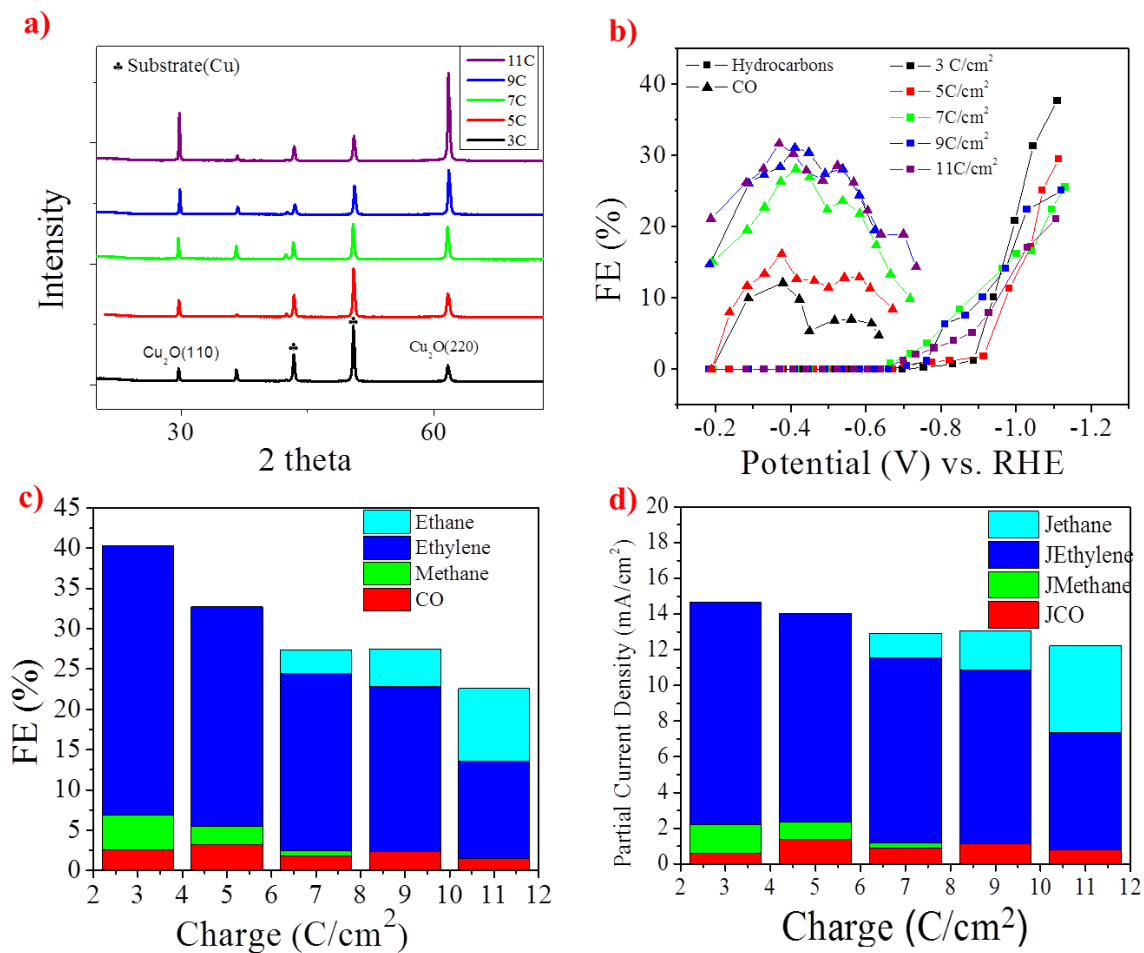


Figure 3

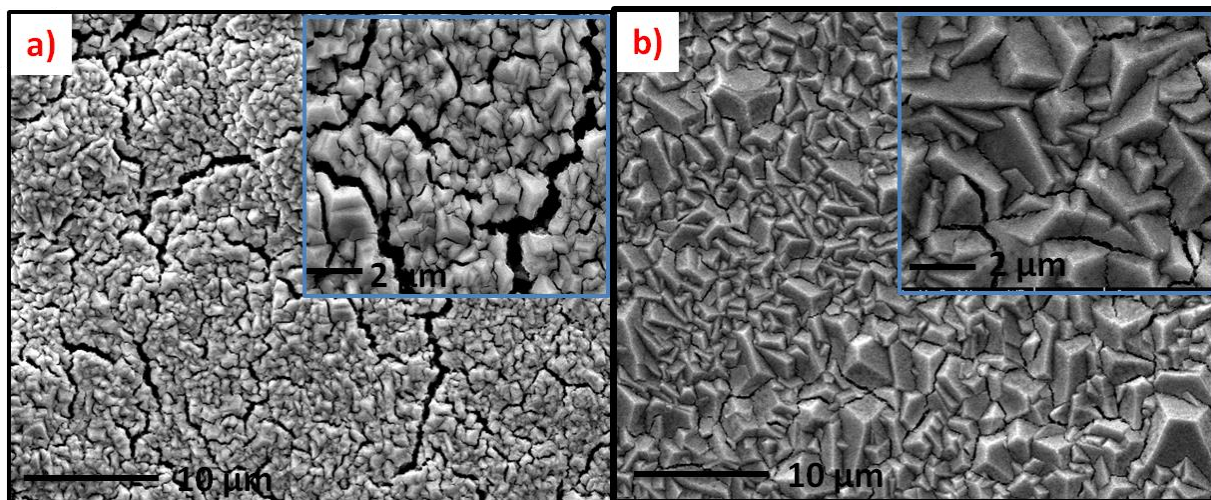


Figure 4

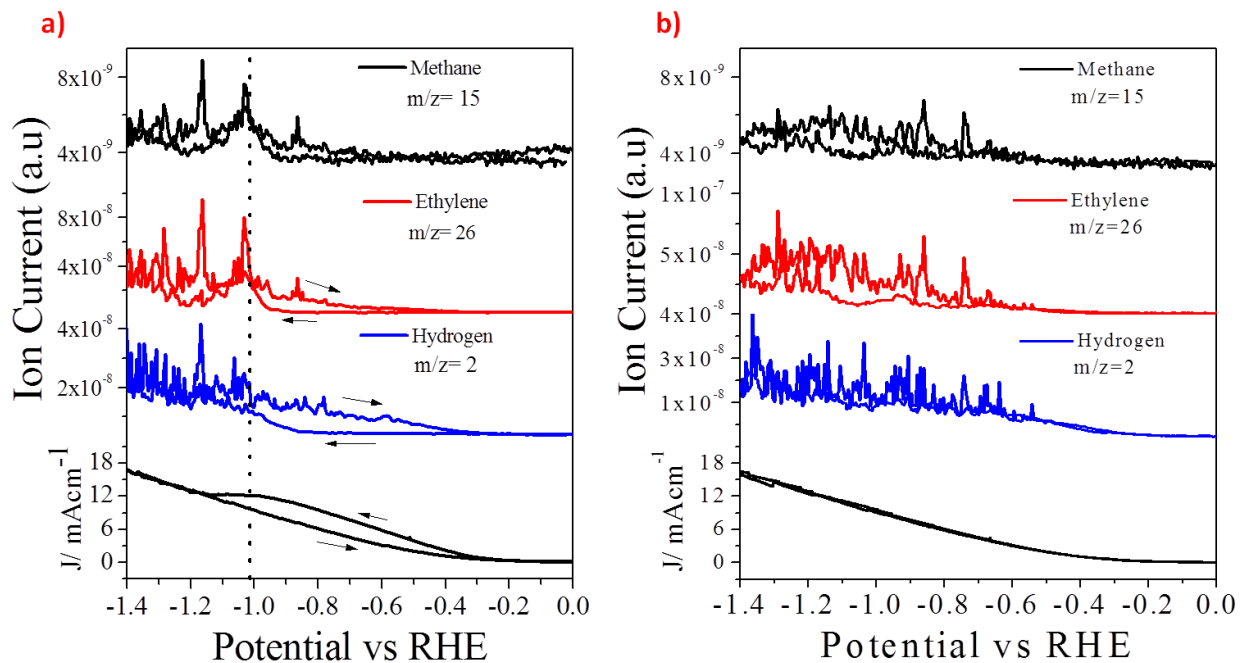
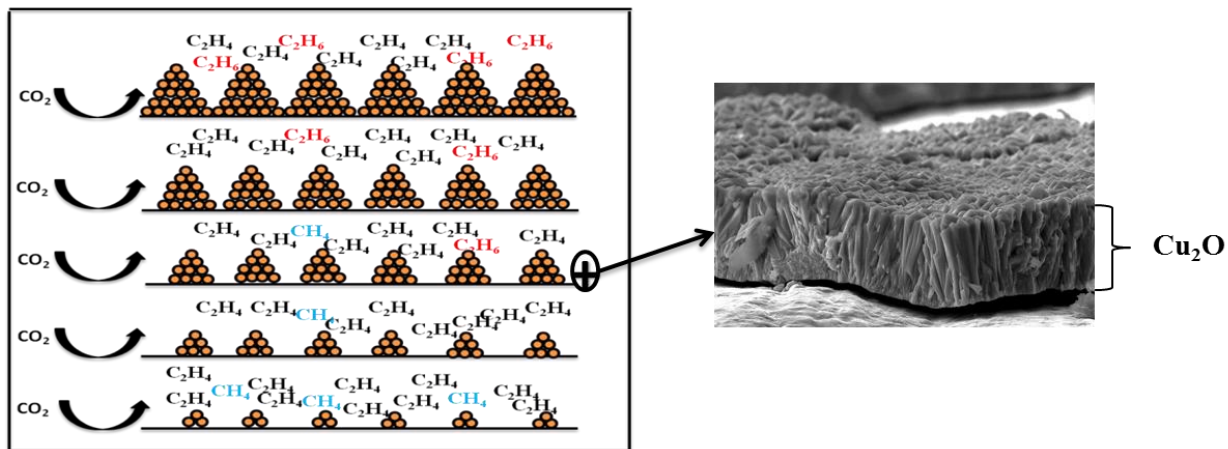


Figure 5



TOC

**Electrochemical CO₂ Reduction on Cu₂O-derived Copper Nanoparticles:
Controlling the Catalytic Selectivity of Hydrocarbons**

Recep Kas,¹ Ruud Kortlever,² Alexander Milbrat,¹ Marc T. M. Koper,² Guido Mul^{1,*} and Jonas Baltrusaitis^{1,*}

¹*PhotoCatalytic Synthesis Group, MESA+ Institute for Nanotechnology, Faculty of Science and Technology, University of Twente, Meander 229, P.O. Box 217, 7500 AE Enschede, The Netherlands*

²*Leiden Institute of Chemistry, Leiden University, Einsteinweg 55, P.O. Box 9502, 2300 RA Leiden, The Netherlands*

ABSTRACT: The catalytic activity and hydrocarbon selectivity in electrochemical carbon dioxide (CO₂) reduction on cuprous oxide (Cu₂O) derived copper nanoparticles is discussed. Cuprous oxide films with [100], [110] and [111] orientation and variable thickness were electrodeposited by reduction of copper (II) lactate on commercially available copper plates. After initiation of the electrochemical CO₂ reduction by these oxide structures, the selectivity of the process was found to largely depend on the parent Cu₂O film thickness, rather than on the initial crystal orientation. Starting with thin Cu₂O films, besides CO and hydrogen, selective formation of ethylene is observed with very high ethylene-to-methane ratios (~8 to 12). In addition to these products, thicker Cu₂O films yield a remarkably large amount of ethane. Long term Faradaic efficiency analysis of hydrocarbons shows no sign of deactivation of the electrodes after 5 hours of continuous experiment. Online mass spectroscopy studies combined with X-ray diffraction data suggest the reduction of the Cu₂O films in the presence of CO₂, generating a nanoparticulate Cu morphology, prior to the production of hydrogen, CO, and hydrocarbons. Optimizing coverage, number density and size of the copper nanoparticles, as well

as local surface pH, may allow highly selective formation of the industrially important product ethylene.

*corresponding authors: j.baltrusaitis@utwente.nl, g.mul@utwente.nl

INTRODUCTION

Carbon dioxide (CO₂) is the thermodynamically stable product of most hydrocarbon feedstock combustion processes and a significant contributor to the greenhouse effect.¹ The accumulation of CO₂ in the atmosphere has an impact on climate change and could threaten the environment and eventually the worldwide economy.^{2, 3} The conversion of CO₂ into useful products and chemicals is thus a very attractive research area.^{4, 5} A currently proposed approach is the electrocatalytic reduction of CO₂ where the electrons are supplied from renewable energy sources, such as photovoltaics, wind and blue energy.⁶⁻⁸ However, CO₂ reduction into fuels is anticipated to be very challenging, due to the necessary multiple number of proton-coupled electron transfer steps.⁹

Many polycrystalline metals have been analyzed for their activity towards electrocatalytic CO₂ reduction.¹⁰ Among the metal electrodes, copper is the most extensively studied since it is the only metal capable of producing hydrocarbons from CO₂ with reasonable Faradaic efficiencies (FE) in aqueous solutions at ambient conditions of temperature and pressure.^{11, 12} However, high overpotentials required for the activation of CO₂ and rapid degradation of the catalytic activity are the major obstacles for commercializing the process.^{13, 14} Even though the deactivation of the catalytic activity is reported to be suppressed by preparing electrolytes via pre-electrolysis or applying anodic pulses,^{14, 15} the reproducibility and compatibility of these preparation steps are not appropriate for large scale application. The key issue in the current state of electrocatalytic CO₂ reduction is to find a stable and robust cathode material that could selectively convert CO₂ and H₂O to useful products at low overpotentials.¹⁶ Energy efficient processes at low overpotentials were reported using ionic liquids as solvent¹⁷ or pyridine as additive¹⁸. Besides low current densities reported in these studies, the effects of the solvents on the electrolyzer are

unknown. The modification of polycrystalline copper surfaces with different structures might allow for a stable electrode performance in aqueous solutions and energy efficient transformation routes towards energy dense products.¹⁹

Growing oxide films on top of a metallic surface is a widely used method of producing structured electrode surfaces.^{20, 21} Methanol was anticipated to form on cuprous oxide (Cu_2O) coated Cu surfaces.^{22, 23} However, deactivation of these electrodes for methanol production after short reaction times suggests conversion of the oxide films in the process. Recently, thermally produced thick oxide films were reported to decrease the overpotential of product formation without losing activity for extended electrolysis time.^{19, 24-26} The CO_2 electrocatalytic reduction process on these copper oxide films was proposed to take place on *in-situ* produced copper oxide nanoparticles during cathodic reconstruction of the Cu_2O oxide films. The selectivity of the thick films was predominantly towards carbon monoxide (CO) and formic acid at low potentials, contrary to thin oxide films which mainly produced methanol.¹⁹ Although several aspects of the thermal-oxide derived electrodes have been validated by Kanan and coworkers, the selectivity towards hydrocarbons, and mechanistic pathways explaining formation thereof, have not been extensively described.

In this study, the performance of electrochemically produced Cu_2O coated copper substrates towards CO_2 reduction is evaluated in terms of selectivity, activity and long term stability. Cu_2O films with surfaces exposing different crystal facets were prepared via controllable, facile, well established electrochemical methods, and the resulting catalytic performance was evaluated using gas chromatography and online electrochemical mass spectroscopy (OLEMS). The effects of the crystal orientation, oxidation state and thickness of the films on the resulting CO_2

electrocatalytic reduction product selectivity will be extensively discussed, with focus on the formation of methane, ethylene and ethane.

EXPERIMENTAL SECTION

Chemicals, materials and Cu₂O film deposition. All working solutions were prepared and all glassware cleaned using deionized water (Millipore MilliQ, 18.2 MΩ cm). Cuprous oxide films were electrodeposited onto copper plates (Alfa Aesar, 99.99 %) from Cu²⁺ containing solutions prepared using 0.4 M CuSO₄ (Sigma Aldrich, ≥99%) and 3 or 4 M lactic acid (Sigma Aldrich) at 60 or 70 °C, according to the procedures described elsewhere.²⁷ The pH of the solution was carefully adjusted between 9 and 12 using solid NaOH (Sigma Aldrich, 98%) and a 1 M NaOH solution. Copper plates were prepared by mechanical polishing using emery paper, followed by cleaning ultrasonically in ethanol and water. The electrodeposition was conducted in a standard three-electrode cell where platinum mesh and Ag/AgCl in 3M NaCl served as counter and reference electrodes, respectively. Galvanostatic deposition was performed at 0.8 and 2 mA/cm² using a potentiostat/galvanostat (PAR, Versastat 3). Specifically, the crystalline morphology was controlled by adapting experimental parameters. Cu₂O films were deposited using a molar lactic acid (LA)/Cu²⁺ ratio of 10 and 7.5 at pH 12 and pH 9, respectively. The deposition times of the films varies depending on the current density applied. Deposition was continued until a total charge of 7 C/cm² was passed through the cell for all samples. Series of [110] oriented films were prepared by passing a variable amount of total electrical charge through the electrochemical cell, ranging from 3 to 11 C/cm² to control the thickness of the film.

The crystalline phase of the films was determined using X-ray diffraction (a Bruker D2 Phaser, equipped with a Cu-K α radiation source operating at 30 kV and 10 mA). Electron microscopy images were taken using a Phillips FEI XL30 FEG-ESEM and FEI Sirion HR-SEM.

Electrochemical CO₂ reduction experiments. Electrochemical CO₂ reduction was carried out in a glass cell using a three electrode assembly at room temperature and pressure. 85 ml of 0.1 M KHCO₃ (Sigma Aldrich, 99.99%) was used as electrolyte at pH 6.8, as obtained after saturation with CO₂ (Linde Gas Benelux 99.99%). Pt mesh was used as counter electrode and was separated from the working electrode using a proton exchange Nafion 112 membrane (Sigma Aldrich). Ag/AgCl in 3M NaCl was used as a reference electrode and potentials were recalculated with reference to the Reversible Hydrogen Electrode (RHE) scale after the experiments. CO₂ was continuously purged at a rate of 20 ml/min for 30 minutes before each experiment, to attain saturation of the electrolyte. Then the flow rate was decreased to 5 ml/min, during which electrochemical reduction was conducted. The continuously purged headspace of the reactor was approximately 45 ml and the reactor effluent sampled directly via gas chromatography (GC) once every 6 min. The GC was equipped with two different columns (ShinCarbon 2m micropacked column and Rtx-1) for simultaneous separation of CO, CO₂, H₂ and hydrocarbons. A thermal conductivity detector (TCD) and flame ionization detector (FID) were used to perform the quantitative analysis of the gas phase products. The time needed to reach the steady state concentration was approximately 40 minutes (see Figure S11), so all experiments were conducted for at least 1 hour before gas phase measurement. A control cathodic experiment was conducted at -1.1 V vs RHE by purging N₂ through the reactor since the decomposition of organics associated with the electrodeposition can also yield hydrocarbons.²⁸ No hydrocarbon or CO formation were detected in the absence of CO₂. Liquid

products formed during the electrolysis were analyzed off line using High Performance Liquid Chromatography (HPLC) (Prominence HPLC, Shimadzu; Aminex HPX 87-H column, Biorad).

Electrochemical Surface Area Measurements: The relative surface roughness factors of the nanoparticulate surfaces were calculated by measuring their capacitance values in 0.5 M H₂SO₄. Pt mesh was used as a counter electrode and Ag/AgCl was used as reference electrode. After reducing the layers in 0.1 M KHCO₃, cyclic voltammetry (CV) curves were obtained with different scan rates in the potential region where non-faradaic processes occur. The slope of the current density vs scan rate yielded the capacitance value which was normalized to bare copper, to obtain the surface roughness factors ((Figures SI2a and SI2b).

OLEMS measurements: Online electrochemical mass spectroscopy (OLEMS) was used to detect gaseous products formed during CO₂ reduction.^{29, 30} The products were collected with a small hydrophobic tip that was positioned close to the electrode (about 10 μm) with the aid of a camera. The tip was constructed as a porous Teflon cylinder with a diameter of 0.5 mm and an average pore size of 10-14 μm in a Kel-F holder. The tip was connected to the mass spectrometry chamber with a PEEK capillary. Before experiments the tip was cleaned in a solution of 0.2 M K₂Cr₂O₇ in 2 M H₂SO₄ and rinsed thoroughly with Millipore water. A secondary electron multiplier (SEM) voltage of 2,400 V was used for detection of products in a Balzers quadrupole mass spectrometer, except for hydrogen where a SEM voltage of 1,200 V was used. The products were measured while changing the potential of the electrode from 0.0 V to -1.4 V vs. RHE and back at 1 mV s⁻¹.

RESULTS AND DISCUSSION

Electrochemical Deposition of Cu₂O Films. SEM images and the corresponding XRD patterns of as prepared Cu₂O films are shown in Figures 1a-d. The XRD patterns acquired clearly indicate that the crystals obtained are preferentially oriented in either [100], [110] and [111] directions, depending on the applied synthesis conditions. The films grown at pH 12 with a current density of 0.8 mA/cm² exhibit triangular pyramids oriented in the [110] direction where the (100) and (010) facets are exposed.³¹ Increasing the current density to 2 mA/cm² at pH 12 favors the growth in [100] directions with three-faced pyramids, where the sides of the pyramids expose (111) facets.³² At pH 9 the morphology of the crystals evolved to four sided pyramids oriented in the [100] direction exposing (111) facets.²⁷

Electrodeposition of Cu₂O films has been extensively studied and well established from Cu²⁺ solutions in the presence of the surfactants and complexing agents, such as sodium dodecyl sulfate, or lactic acid.³³⁻³⁵ Formation of [111] and [100] oriented films was studied previously extensively,^{32, 36-38} whereas [110] oriented films were reported in a couple of studies and were found to be stable in a very narrow pH range.³¹ Our attempts to reproduce [110] oriented films were successful, but the orientation of the films was found to be different at increasing thickness, which is most likely due to a change in pH and copper concentration during the electrodeposition.³² Nevertheless, we found that increasing the amount of lactic acid at pH 12 yields [110] oriented films with low current densities in a reproducible way.

Electrochemical CO₂ reduction in 0.1 M KHCO₃ on different facets of Cu₂O films. The distribution of the gaseous products obtained during the CO₂ electrochemical reduction at a cathodic potential of -1.1 V vs RHE is presented in Figure 1e. It can be seen that only minor differences exist in the FE of the gaseous products between the different predominant crystal

oriented films. In particular, CO, methane, ethylene and some ethane were gaseous products observed of CO₂ electrochemical reduction. CO desorbs from the surface and is a well-known intermediate for the formation of ethylene and methane.¹⁰ Ethylene was the major product among the hydrocarbons for all of the samples with a small variation in ethylene/methane ratio observed. Ethane formation was detected with low FE for all of the samples investigated. Unfortunately, we were not able to compare the data to the performance of polycrystalline copper electrodes: complete deactivation of polycrystalline copper was observed, before steady state was reached (the reactor was operated as CSTR).

XRD patterns obtained of the samples after the CO₂ experiments were acquired and show that only diffraction lines due to metallic copper are present (See Figure SI3). Thus, in the potential range applied here for CO₂ electrochemical reduction (-0.2V to -1.1 V vs RHE), none of the Cu₂O films were stable, and reduced to metallic copper. The SEM images of the samples shown in Figure 2a-c signify different microscopic morphology of the films obtained after the reduction process, when compared to that before the reduction. When compared to those in Figure 1, the smooth surfaces of the pyramids roughened and the films cracked at the intersection of the pyramids. The higher magnification insets in Figure 2 show that pyramids are now composed of spherical nanometer sized copper domains. As it will be established further using OLEMS studies, CO₂ reduction apparently did not proceed on Cu₂O, but rather on *in situ* formed metallic copper nanoparticles. Even though there is no distinct difference between the samples in terms of their corresponding product selectivity as a function of initial Cu₂O orientation, suggesting the structure of the *in situ* formed copper nanoparticles is not much different, the observed high ethylene selectivity of the electro-catalytically active copper surfaces is distinctly different from the selectivities previously reported for polycrystalline copper, and oxide derived copper

nanoparticles.^{12, 19, 26} Electro-polished polycrystalline copper is well known to produce methane as the major product within the investigated potential range,¹³ while ethane was reported to be a dominant product on copper derived from thermally formed oxide films.¹⁹ Further, in agreement with our product distribution, anodically created oxide films were found to lead to formation of predominantly ethylene, but for these films ethane formation was not observed.²⁶ To further analyze the effect of the structure of the oxide derived copper nanoparticle layer on hydrocarbon selectivity, layers with different thickness were prepared and evaluated in electrocatalytic CO₂ reduction.

Electrochemical CO₂ reduction in 0.1 M KHCO₃ on (110) Cu₂O films of increasing thickness. The XRD patterns of a series of [110] oriented Cu₂O films prepared by passing a different amount of total electrical charge through the electrochemical cell, are shown in Figure 3a. It can be seen that the diffraction line due to the [110] plane becomes more predominant as the thickness of the films increases. Likewise, the intensity of the metallic copper diffraction lines from the substrate decreases, as the thickness of Cu₂O films increases. Growth in the [100] and [111] directions has been reported to be restricted to a localized or spotty deposition, suggesting growth of our films is more homogeneous to explain the observed preferred [110] crystal orientation of our films.³⁷ CO₂ reduction on the thus prepared electrodes was performed in the potential range between -0.2 and -1.1 V vs RHE. A plot of CO and hydrocarbon FE (%) vs. the applied cathodic potential is shown in Figure 3b. For the samples having higher initial oxide thicknesses, CO formation starts at very low overpotentials (~-0.1 V) and reaches a maximum between -0.3 and -0.5 V vs RHE. These observations are consistent with findings on thermally induced oxide derived films of copper.¹⁹ At higher applied potentials, the FE towards CO decreases, and hydrocarbon products start to evolve with onset potentials between -0.65 and

-0.75 V vs RHE. The change in hydrocarbon product distribution (FE (%)) at cathodic potential of -1.1 V vs RHE as a function of thickness is given at Figure 3c. A major observation is that the distribution of the hydrocarbon products changes distinctively from methane to ethane, CO being relatively constant, and ethylene continuously decreasing. No deactivation towards the hydrocarbon production was observed for the thinnest samples over the course of 5 hours (Figure SI4), as compared to polycrystalline copper which was found to rapidly deactivate within 40 minutes.¹⁴

SEM images of the thinnest (3 C/cm²) and the thickest (11 C/cm²) Cu₂O samples after the electrochemical CO₂ reduction process are shown in Figures 4a and b, respectively. The morphology of the thinnest [110] oriented films is not well pronounced, whereas thicker films show characteristic triangular pyramid morphology. It can be seen that the increase in the initial oxide films thickness increases the coverage of the pyramids, which are again composed of the aggregated copper nanoparticles after reduction. As the thickness of the initial oxide films increases, the size of the cracks between the overlapping pyramids decreases and the individual pyramids start to form continuous films. Sample surface roughness, relative to that of bare copper, was measured and is tabulated in Table 1. As the oxide layer thickness increases, the roughness factors of the *in situ* formed nano particulate copper surface increase as well, ranging from 11 for an oxide derived layer produced at 3 C/cm² to 65 for an oxide derived layer produced at 11 C/cm². Additionally, the increase in the geometrical current density as a function of initial oxide layer thickness confirms the increase in surface roughness (Figure SI5).

Even though the FE of the hydrocarbon products clearly decreases for increasing layer thickness (i.e. the selectivity decreases), the overall current density increases (Figure SI5), and hence the decrease in partial current density values (calculated by the product of the overall current density

and the sum of the FE of the gaseous products) is not as significant (Figure 3d). In other words, the production rate of hydrocarbons (and CO₂ conversion rate) only slightly decreases (reflected by the change from 15 to 12 mA/cm²).

Liquid product analysis for the thinnest sample (3 C/cm²), indicated the formation of formic acid as a non-volatile product (Figure SI6). The Faradaic efficiency amounts to approximately 20%. We have not evaluated the formic acid formation for the other samples, and will focus the remainder of the discussion on the changes in volatile hydrocarbon composition.

Extensive research on the relation between the structure of Copper surfaces and the product composition exists. Single crystal copper electrodes by Hori *et al.* showed that stepped surfaces result in higher selectivity towards ethylene.³⁹ Introducing (111) steps on to the (100) basal plane increases the formation of ethylene over methane with the highest ethylene/methane ratio of ~14 observed on Cu(711).⁴⁰ On the other hand, the width of the Cu(100) terraces is suggested to be a decisive factor towards ethylene formation on stepped copper surfaces.⁴¹ Recently Schouten *et al.* proposed that ethylene formation takes place at low overpotentials on Cu(100) through adsorption of CO dimers, whereas at higher potentials both ethylene and methane formation takes place on (100) and (111) facets via a shared intermediate.⁴² Although we appreciate the effect of surface exposed planes on selectivity, we conclude on the basis of the very similar results obtained for the different Cu₂O morphologies that the structure of the Cu nanoparticles *in situ* formed in electrochemical CO₂ reduction are not profoundly different. To explain the dramatic changes in selectivity due to increasing layer thickness thus has to have an alternative origin.

Importantly, the CO dimerization mechanism on Cu(100) is enhanced in alkaline media.⁴³ Therefore, ethylene formation is suggested to take place at conditions of high (local) pH.⁴¹ The trend of product selectivity towards hydrocarbons observed here with increasing oxide layer thickness is then explained by local changes in pH during the electrolysis. Gupta *et al.* modeled the local pH changes during the electrochemical CO₂ reduction in KHCO₃ solutions.⁴⁴ The local pH near the electrode surface during electrolysis is higher than the bulk value and depends on the applied current density, electrolyte concentration, and stirring speed. The increase in surface roughness and the geometrical current density of the Cu films investigated here, likely lead to an increase in local pH due to the observed increase in hydrogen production (Figure SI7) consuming H⁺. The increasing hydrogen FE as a function of film thickness at potentials above -1.0 V vs RHE is in agreement with the increasing current caused by the presence of the higher surface area, providing additional surface sites for hydrogen evolution. The formation of methane and ethylene have been reported to have a distinctly different pH dependence due to the difference in the involvement of protons in their rate limiting step.^{41, 45} As a result, at higher (local) pH, the formation of ethylene from the CO intermediate is preferred over the formation of methane. The increase in the current density of hydrogen evolution reaction and local pH changes could therefore possibly explain the decrease and disappearance of methane with the increasing oxide thickness.

Ethane formation so far has only been observed on very rough surfaces, such as electrodeposited foam-like structures,⁴⁶ as well as thermally produced oxide films reduced by hydrogenation or electrochemically.^{19, 45} Recent calculations on C-C coupling on Cu(211) surfaces suggest the kinetic barriers for the coupling are strongly influenced by the degree of the adsorbed CO hydrogenation.⁴⁷ These kinetic barriers tend to decrease with increasing degree of the surface

bound CO hydrogenation, which can favor ethane. However, the absence of methane formation on the electrodes where ethane is formed suggest the formation is unlikely to occur via the formation of adsorbed $-\text{CH}_3$, which is proposed as an intermediate for methane formation.⁴⁸ The hydrogenation appears to take place after the C-C coupling, such as further reduction of ethylene, in agreement with ethane being formed at the expense of ethylene. Attempts to reduce ethylene on the thickest initial oxide layer electrode directly were unsuccessful due to the broadening and saturation of the ethylene peak in the gas chromatogram, which eventually overlapped with the ethane peak position. However, preliminary OLEMS experiments have demonstrated the hydrogenation of ethylene over Cu surfaces is feasible; results to be published elsewhere.

In order to obtain deeper insight into the role of the cuprous oxide on CO_2 electrochemical reduction, OLEMS studies were conducted on the [111] and [100] oriented films of different thickness. All of the samples prepared by passing 1 to 5 C/cm^2 showed similar catalytic behavior, when analyzed with OLEMS. Therefore, only the 5 C/cm^2 sample is discussed in detail. The CV graphs obtained are shown in Figure 5, together with the corresponding mass spectroscopy data. Specifically, the very first cathodic sweep is shown in Figure 5a, whereas the following, second sweep, is shown in Figure 5b. A clear reductive wave can be observed in Figure 5a, which is absent in Figure 5b. This is due to the decomposition of electrodeposited cuprous oxide, which starts around -0.3 V vs RHE. Since this process always proceeds during the initial cathodic sweep, all electrochemical CO_2 reduction proceeds on the newly *in situ* formed metallic copper particles and not on as-deposited Cu_2O , in agreement with our data presented earlier. The dashed vertical line in Figure 5a corresponds to the potential where a total charge of 5 C/cm^2 was passed through the electrode for the reduction of the films. Importantly, in the first and the consecutive forward scans no mass fragments corresponding to hydrogen and ethylene were

detected, until reaching the conditions needed for the reduction of the films. At the same potentials, appreciable amount of hydrogen and ethylene is produced during the reverse scan, as well as the second and the following sweep cycles.

Copper oxides are known to form spontaneously on copper when exposed to air or electrolyte solution.⁴⁹ Intentionally formed Cu_2O films on copper have been reported to yield methanol with very high FE.^{23, 50} However, the catalytic activity of these degrades quickly, which is attributed to the decomposition of cuprous oxide to copper, and methanol is considered to be only formed during the reduction of these oxide films. Further, the initial composition of the copper oxide electrocatalyst surface and its transformations during the reduction process are not exactly known. Spectroscopic analysis of spent CO_2 electroreduction electrodes indicate the presence of Cu(I) and Cu(II) oxides after the reaction,⁵⁰ but *in situ* analysis is required to verify the existence of the oxide films during the electrocatalytic process. Using OLEMS, no noteworthy amount of methanol was detected from the samples evaluated here. This once again suggests that gaseous CO_2 electrocatalytic reduction products is governed by the copper metal formed from the Cu_2O films during *in situ* transformations.

Conclusions

This research highlights the selectivity in electrocatalytic CO_2 reduction of copper nanoparticles derived from different Cu_2O morphologies and surface coverages. The orientation of electrodeposited Cu_2O ([110], [111] and [100]) has only a minor effect on the product selectivity. The initial oxide thickness, however, strongly influences the selectivity of the electrocatalytic process. Specifically, OLEMS studies show that the Cu_2O reduction itself seems to be highly favored, when compared to CO_2 reduction or water splitting, since no products were detected by

online mass spectroscopy on as deposited Cu_2O . Further, the catalytic behavior is predominantly determined by layer thickness associated local pH changes, impacting the hydrocarbon selectivities. The optimum number density of nanoparticles with the combination of the right electrolyte (pH) can open up routes for highly selective ethylene formation via electrochemical reduction of CO_2 in reactors. In addition, gas diffusion electrodes or high pressure can be used to improve CO_2 mass transport.

Acknowledgements

This work is supported by NanoNextNL, a micro and nanotechnology consortium of the Government of the Netherlands and 130 partners. We would like to thank Dr. Youngkook Kwon from Leiden University for mass spectrometry measurements. We would also like to thank Dr. Engin Karabudak for fruitful discussions.

Notes and references

Electronic Supplementary Information (ESI) available: details on Faradaic efficiency calculations, steady state reactor conditions, XRD of reduced Cu_2O coatings, long term stability analysis at constant potential, FE of H_2 evolution and CV curves of different thickness oxides. See DOI: 10.1039/b000000x/

1. D. M. D'Alessandro, B. Smit and J. R. Long, *Angew. Chem. Int. Ed.*, 2010, **49**, 6058-6082.
2. S. Solomon, D. Qin, M. Manning, Z. Chen, M. Marquis, K. Averyt, M. Tignor and H. Miller, Contribution of Working Group I to the Fourth Assessment Report of the Intergovernmental Panel on Climate Change, Cambridge University Press, UK and New York, NY, USA, 2007.
3. M. M. Halmann and M. Steinberg, *Greenhouse gas carbon dioxide mitigation: science and technology*, CRC press, 1999.
4. S. K. Ritter, *Chem. Eng. News*, 2007, **85**, 11-17.
5. G. A. Olah, G. S. Prakash and A. Goepfert, *J. Am. Chem. Soc.*, 2011, **133**, 12881-12898.
6. R. E. Blankenship, D. M. Tiede, J. Barber, G. W. Brudvig, G. Fleming, M. Ghirardi, M. R. Gunner, W. Junge, D. M. Kramer, A. Melis, T. A. Moore, C. C. Moser, D. G. Nocera, A. J. Nozik, D. R. Ort, W. W. Parson, R. C. Prince and R. T. Sayre, *Science*, 2011, **332**, 805-809.

7. C. Graves, S. D. Ebbesen, M. Mogensen and K. S. Lackner, *Renew Sust. Energy Rev.*, 2011, **15**, 1-23.
8. G. Mul, C. Schacht, W. P. van Swaaij and J. A. Moulijn, *Chem. Eng. Process.*, 2012, **51**, 137-149.
9. B. Kumar, M. Llorente, J. Froehlich, T. Dang, A. Sathrum and C. P. Kubiak, *Annu. Rev. Phys. Chem.*, 2012, **63**, 541-569.
10. Y. Hori, in *Modern aspects of electrochemistry*, Springer, 2008, pp. 89-189.
11. H. Shibata, J. A. Moulijn and G. Mul, *Catal. Lett.*, 2008, **123**, 186-192.
12. Y. Hori, A. Murata, R. Takahashi and S. Suzuki, *J. Am. Chem. Soc.*, 1987, **109**, 5022-5023.
13. M. Gattrell, N. Gupta and A. Co, *J. Electroanal. Chem.*, 2006, **594**, 1-19.
14. Y. Hori, H. Konishi, T. Futamura, A. Murata, O. Koga, H. Sakurai and K. Oguma, *Electrochim. Acta*, 2005, **50**, 5354-5369.
15. R. Shiratsuchi, Y. Aikoh and G. Nogami, *J. Electrochem. Soc.*, 1993, **140**, 3479-3482.
16. D. T. Whipple and P. J. A. Kenis, *J Phys Chem Lett*, 2010, **1**, 3451-3458.
17. B. A. Rosen, A. Salehi-Khojin, M. R. Thorson, W. Zhu, D. T. Whipple, P. J. Kenis and R. I. Masel, *Science*, 2011, **334**, 643-644.
18. G. Seshadri, C. Lin and A. B. Bocarsly, *J. Electroanal. Chem.*, 1994, **372**, 145-150.
19. C. W. Li and M. W. Kanan, *J. Am. Chem. Soc.*, 2012, **134**, 7231-7234.
20. X. Jiang, T. Herricks and Y. Xia, *Nano Lett.*, 2002, **2**, 1333-1338.
21. Y. Chen and M. W. Kanan, *J. Am. Chem. Soc.*, 2012, **134**, 1986-1989.
22. T. Y. Chang, R. M. Liang, P. W. Wu, J. Y. Chen and Y. C. Hsieh, *Mater. Lett.*, 2009, **63**, 1001-1003.
23. M. Le, M. Ren, Z. Zhang, P. T. Sprunger, R. L. Kurtz and J. C. Flake, *J. Electrochem. Soc.*, 2011, **158**, E45-E49.
24. Y. Chen, C. W. Li and M. W. Kanan, *J. Am. Chem. Soc.*, 2012, **134**, 19969-19972.
25. J. Qiao, P. Jiang, J. Liu and J. Zhang, *Electrochem. Commun.*, 2014, **38**, 8-11.
26. W. Tang, A. A. Peterson, A. S. Varela, Z. P. Jovanov, L. Bech, W. J. Durand, S. Dahl, J. K. Nørskov and I. Chorkendorff, *Phys. Chem. Chem. Phys.*, 2012, **14**, 76-81.
27. T. D. Golden, M. G. Shumsky, Y. Zhou, R. A. VanderWerf, R. A. Van Leeuwen and J. A. Switzer, *Chem. Mater.*, 1996, **8**, 2499-2504.
28. C.-C. Yang, Y.-H. Yu, B. van der Linden, J. C. Wu and G. Mul, *J. Am. Chem. Soc.*, 2010, **132**, 8398-8406.
29. R. Kortlever, K. H. Tan, Y. Kwon and M. T. M. Koper, *J. Solid State Electrochem.*, 2013, **17**, 1843-1849.
30. A. H. Wonders, T. H. M. Housmans, V. Rosca and M. T. M. Koper, *J. Appl. Electrochem.*, 2006, **36**, 1215-1221.
31. L. Wang, N. De Tacconi, C. Chenthamarakshan, K. Rajeshwar and M. Tao, *Thin Solid Films*, 2007, **515**, 3090-3095.
32. S. Joseph and P. V. Kamath, *J. Electrochem. Soc.*, 2007, **154**, E102-E106.
33. A. A. V. Julie K. Barton, Eric W. Bohannon, and Jay A. Switzer, *Chem. Mater.*, 2001, **13**, 952-959.
34. S. Joseph and P. V. Kamath, *Solid State. Sci.*, 2008, **10**, 1215-1221.
35. M. J. Siegfried and K. S. Choi, *Adv. Mater.*, 2004, **16**, 1743-1746.
36. M. G. S. Teresa D. Golden, Yanchun Zhou, Rachel A. VanderWerf, Robert A. Van Leeuwen, and Jay A. Switzer, *Chem. Mater.*, 1996, **8**, 2499-2504.
37. A. E. Rakhshani and J. Varghese, *J. Solar Energy Mater*, 1987, **15**, 237-248.
38. W. Septina, S. Ikeda, M. A. Khan, T. Hirai, T. Harada, M. Matsumura and L. M. Peter, *Electrochim. Acta*, 2011, **56**, 4882-4888.
39. Y. Hori, I. Takahashi, O. Koga and N. Hoshi, *J. Phys. Chem. B*, 2001, **106**, 15-17.
40. Y. Hori, H. Wakebe, T. Tsukamoto and O. Koga, *Surf. Sci.*, 1995, **335**, 258-263.
41. K. J. P. Schouten, E. Pérez Gallent and M. T. M. Koper, *ACS Catalysis*, 2013, **3**, 1292-1295.

42. K. J. P. Schouten, Z. Qin, E. P. Gallent and M. T. M. Koper, *J. Am. Chem. Soc.*, 2012, **134**, 9864-9867.
43. F. Calle-Vallejo and M. T. M. Koper, *Angew. Chem. Int. Ed.*, 2013, **52**, 7282-7285.
44. N. Gupta, M. Gattrell and B. MacDougall, *J. Appl. Electrochem.*, 2006, **36**, 161-172.
45. Y. Hori, R. Takahashi, Y. Yoshinami and A. Murata, *J. Phys. Chem. B*, 1997, **101**, 7075-7081.
46. M. R. Gonçalves, A. Gomes, J. Condeço, T. R. C. Fernandes, T. Pardal, C. A. C. Sequeira and J. B. Branco, *Electrochimica Acta*, 2013, **102**, 388-392.
47. J. H. Montoya, A. A. Peterson and J. K. Nørskov, *ChemCatChem*, 2013, **5**, 737-742.
48. K. J. P. Schouten, Y. Kwon, C. J. M. van der Ham, Z. Qin and M. T. M. Koper, *Chemical Science*, 2011, **2**, 1902-1909.
49. M. Pourbaix, *Atlas of electrochemical equilibria in aqueous solutions*, National Association of Corrosion Engineers, 1974.
50. K. W. Frese, *J. Electrochem. Soc.*, 1991, **138**, 3338-3344.

Tables

Table 1. The capacitance values and surface roughness factors of the films as a function of initial thickness of the films.

Figures

Figure 1. SEM images of as deposited Cu₂O films with predominant a) [110], b) [111] and c) [100] orientations. d) X-ray diffraction patterns of Cu₂O films electrochemically deposited on copper substrate. e) FE of gaseous products from CO₂ reduction at -1.1 V vs RHE in 0.1 M KHCO₃ solution for oxides having different crystal orientation.

Figure 2. SEM images of copper nanoparticles obtained after reaction from oxides in the a) [110], b) [111] and c) [100] orientations. Corresponding SEM images are also shown with high resolution images in the inset.

Figure 3. a) The X-ray diffraction patterns of the [110] oriented Cu₂O films prepared by changing the total charge passed through the cell. b) FEs of CO and hydrocarbons at different potentials as a function of initial thickness of the films c) FE and d) partial current density of gaseous products from CO₂ reduction at -1.1 V vs RHE in 0.1 M KHCO₃ solution as a function of initial thickness of the films (FEs of CO are given in a limited potential range for clarity).

Figure 4. SEM image of the [110] oriented a) thinnest (3 C/cm²) and the b) thickest (11 C/cm²) Cu₂O samples after the electrochemical CO₂ reduction.

Figure 5. Ion currents for methane, ethylene, hydrogen probed by OLEMS as a function of applied potential. Cyclic voltammetry curve of oxide films on copper in CO₂ saturated 0.1 M KHCO₃ solution a) first scan b) second scan (scan rate 1 mV s⁻¹). Arrows indicate the forward and backward scans for clarity.

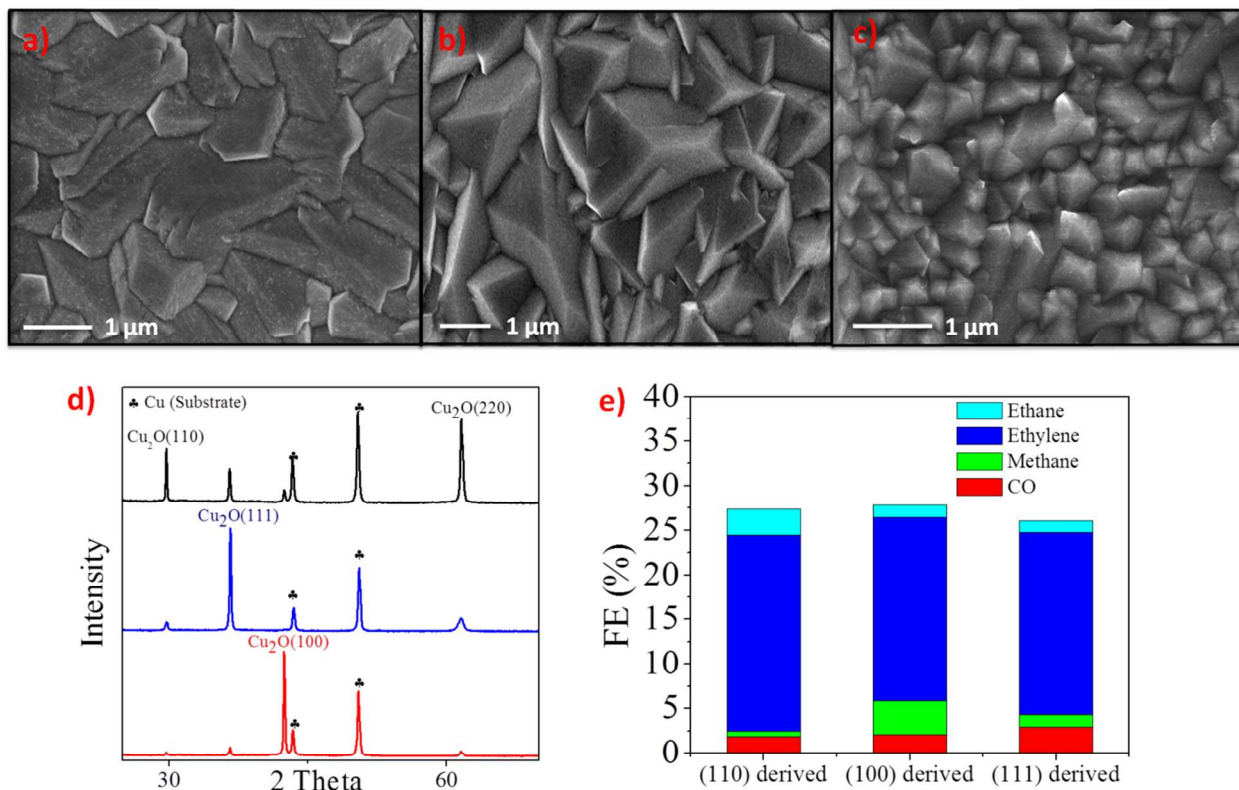


Figure 1

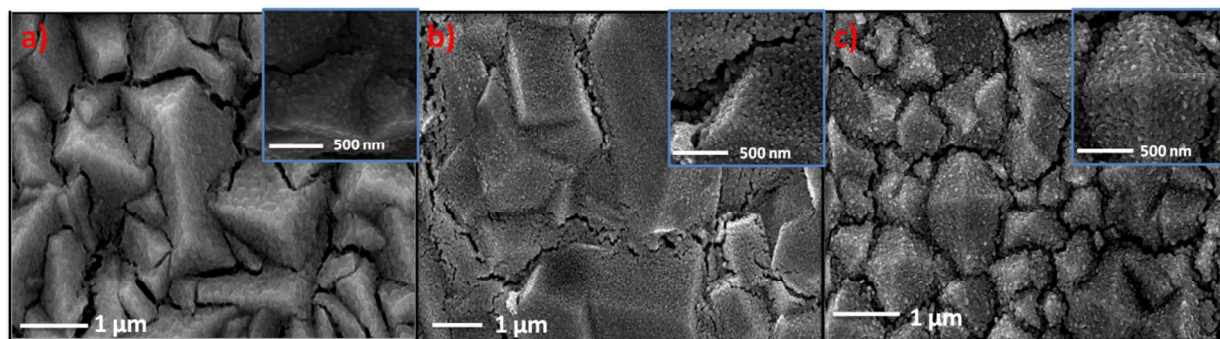


Figure 2

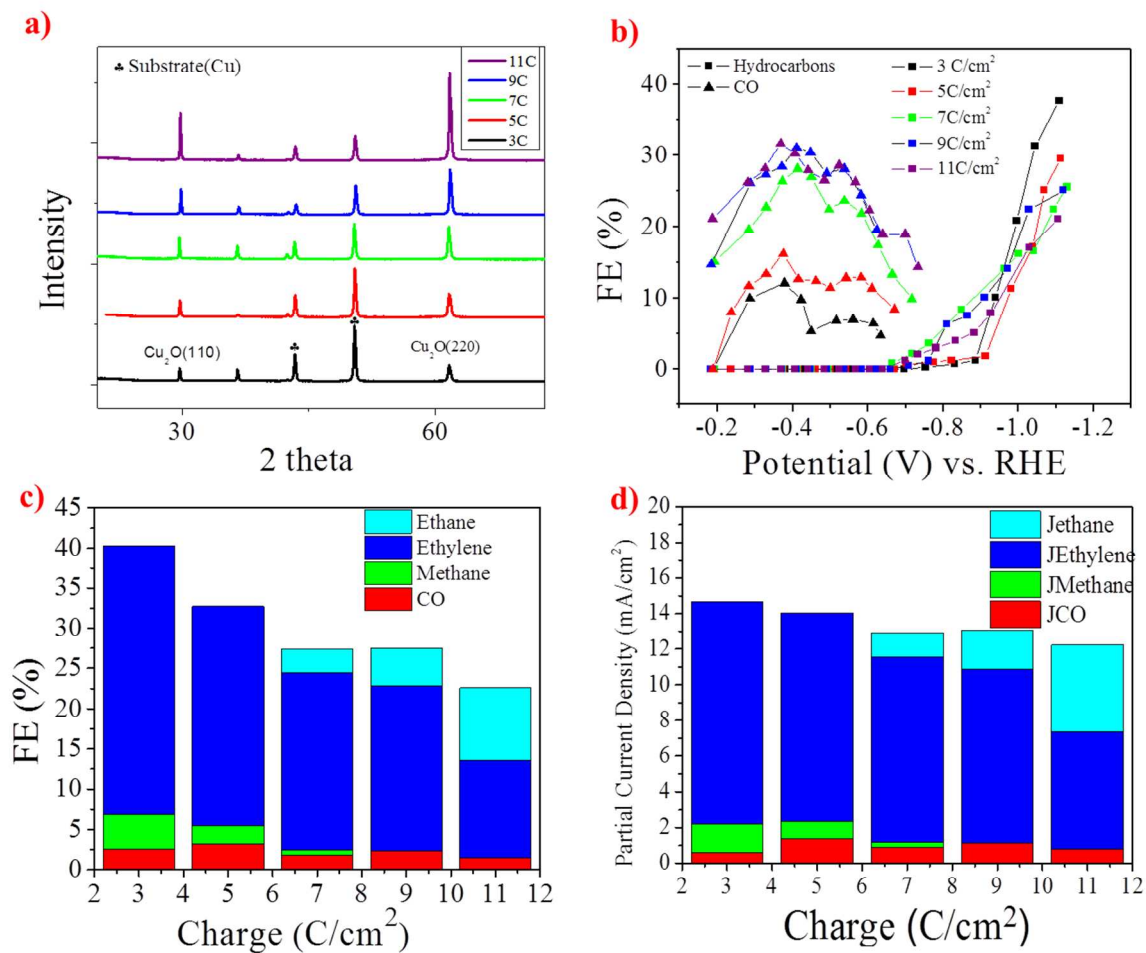


Figure 3

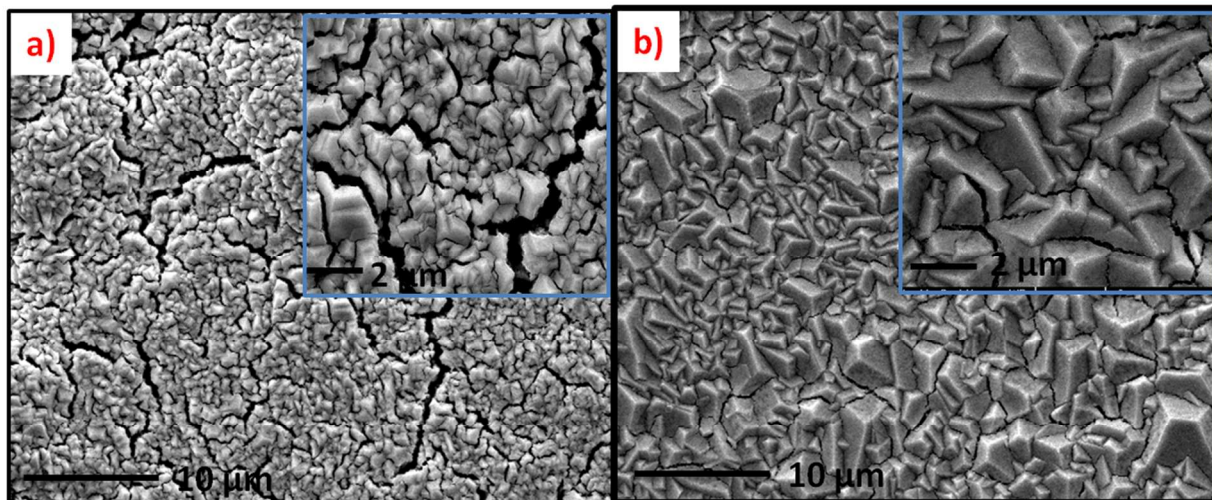


Figure 4

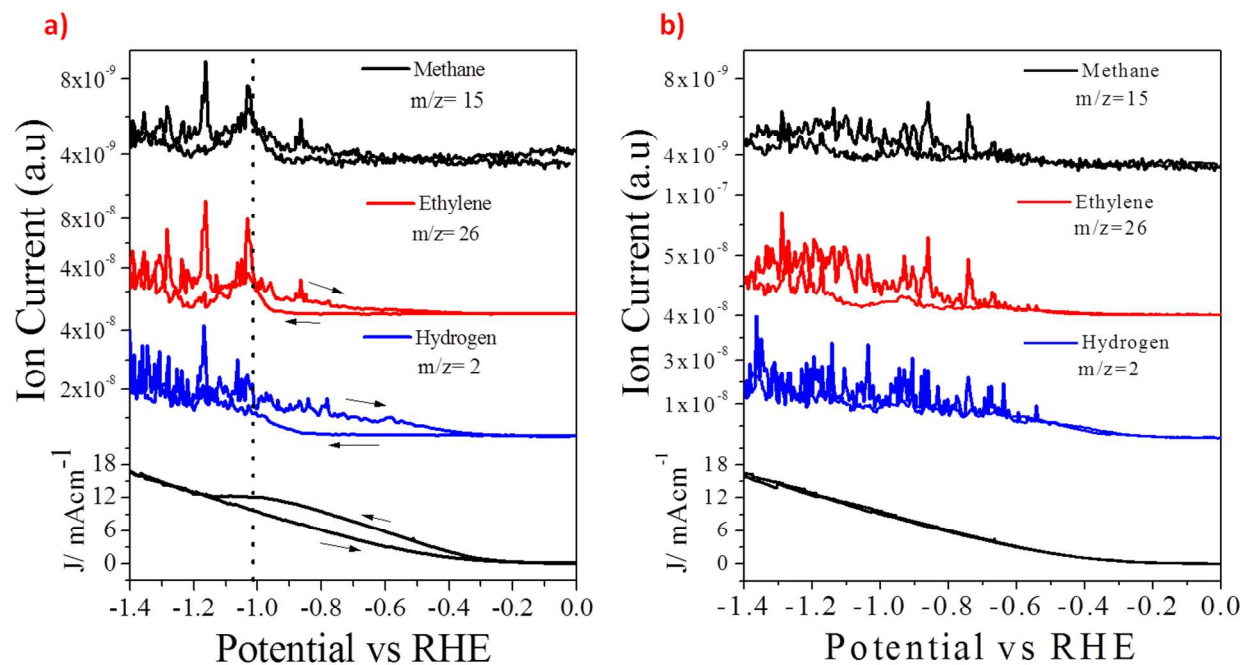
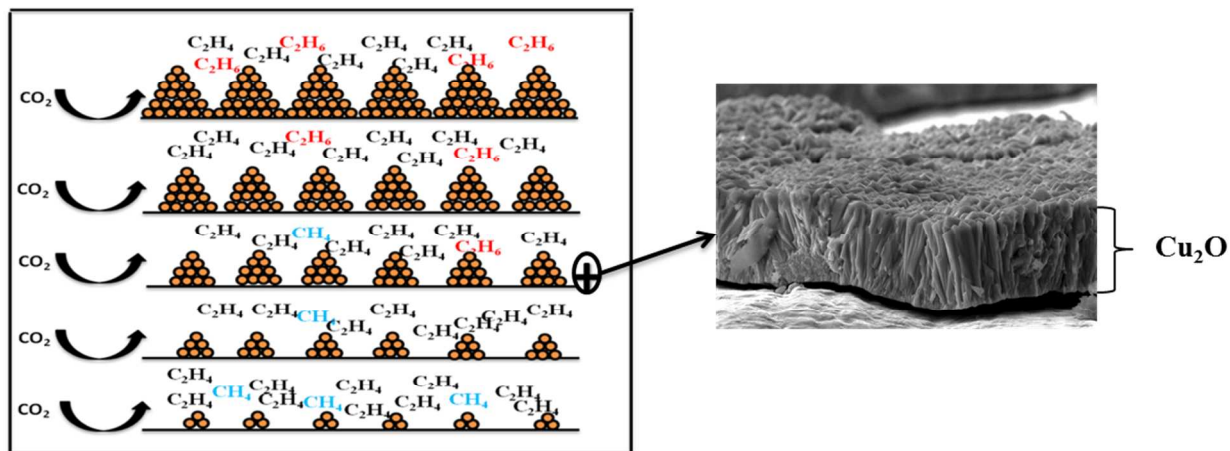


Figure 5



TOC

SUPPORTING INFORMATION

Electrochemical CO₂ Reduction on Cu₂O-derived Copper Nanoparticles:

Controlling the Catalytic Selectivity of Hydrocarbons

Experimental Methods

Faradaic efficiency calculation: The Faradaic efficiency (FE) of the CO₂ electrochemical reduction of products was calculated as

$$FE(\%) = \frac{n_i F \phi_i F_m}{I}$$

where n_i is the number of the electrons needed for CO₂ reduction, F is the Faraday constant, ϕ_i is the volume fraction of the gases, I is the current obtained and F_m is the molar CO₂ gas flow rate. The number of electrons associated with reduction are 2,8,12,14 for formation of CO, methane, ethylene, and ethane, respectively. The volume fraction of the gases is calculated by calibrating the gas chromatogram (GC) using a diluted mixture of gases of known concentrations.

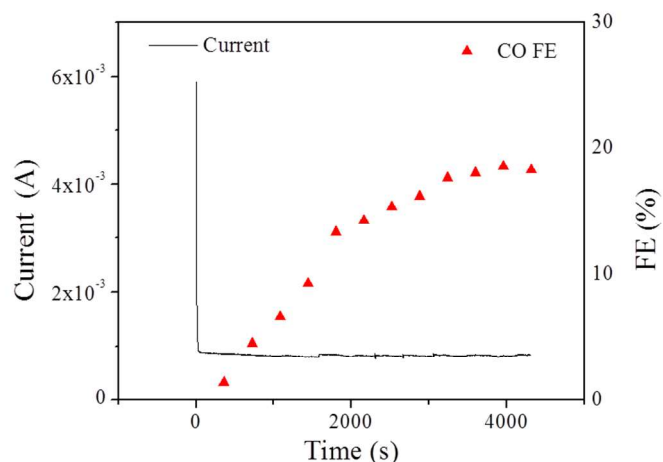


Figure SI1 The transient behavior of the electrochemical reactor at a constant applied potential.

The time needed to reach steady state, applying a flow rate of 5 mL/min, was ~ 40 min, as evident from the trend in CO Faradaic Efficiency. All the CO_2 electrochemical reduction experiments were conducted for at least one hour, and steady state values are reported throughout the manuscript.

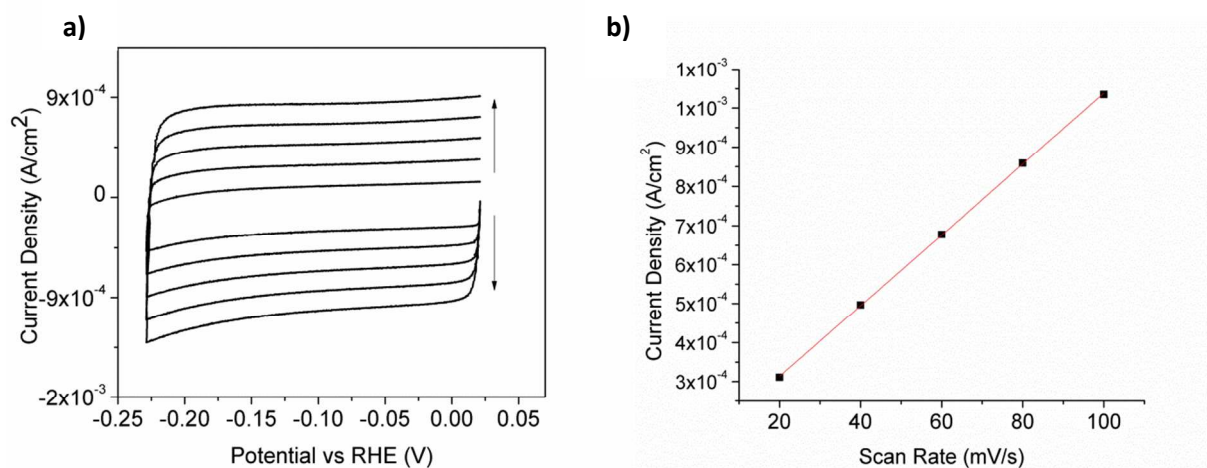


Figure SI2: a) CV curves of a nano-particulate Cu surface derived from an oxide film prepared at 11 C/cm^2 . The arrows indicate the trends induced by an increase in scan rate. b) the current density vs. scan rate plot for the corresponding film.

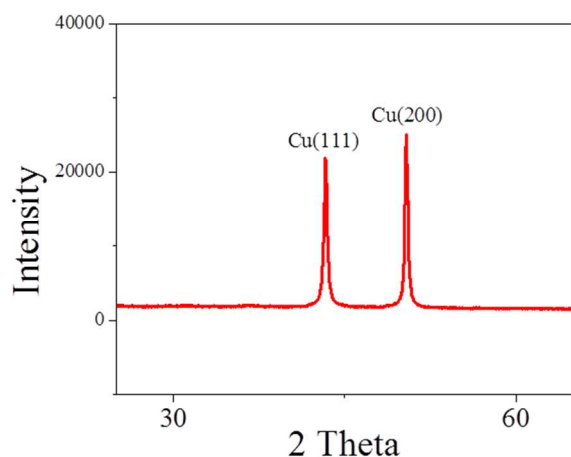


Figure SI3 The X-ray diffraction pattern of coatings after electrochemical reduction at -0.6 V vs RHE.

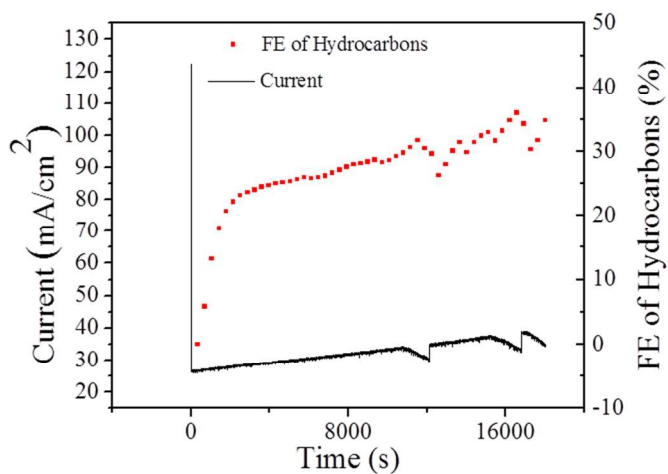


Figure SI4: Long term stability analysis for the thinnest sample (3 C/cm^2) at constant potential. The applied potential varies somewhat in time due to increasing resistance of the solution, in agreement with IR values determined before and after the experiment. The potential at the surface apparently fluctuates between -1.04 and -1.09 V vs RHE during the experiment.

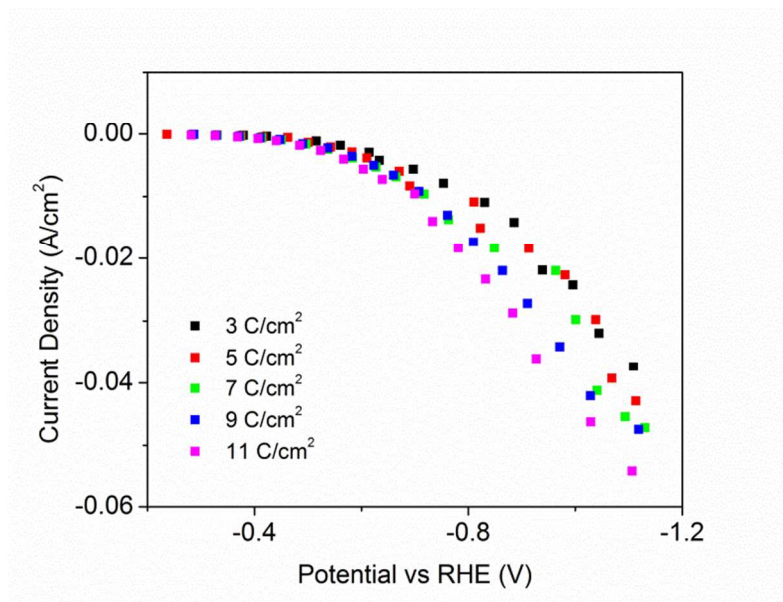


Figure SI5: The stable current density values obtained during electrochemical CO₂ reduction as a function of potential for different thickness of the oxides.

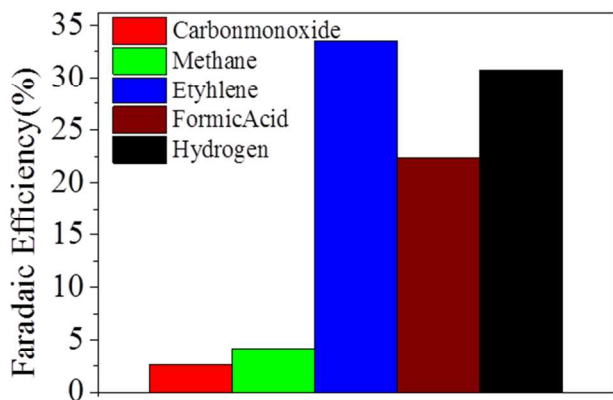


Figure SI6: Product distribution (FE (%)) for the thinnest sample (3C/cm²), including the product Formic Acid, which was dissolved in the electrolyte and determined *ex situ* by HPLC.

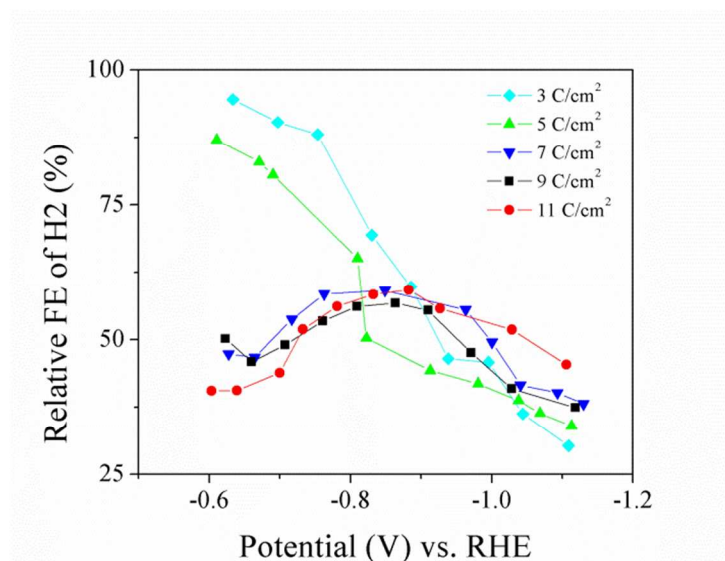
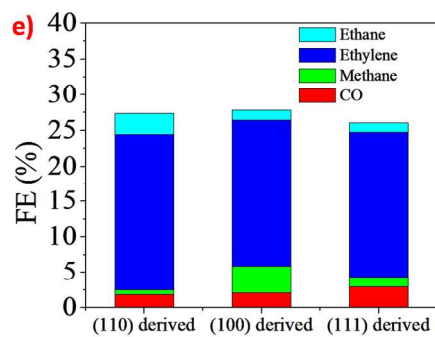
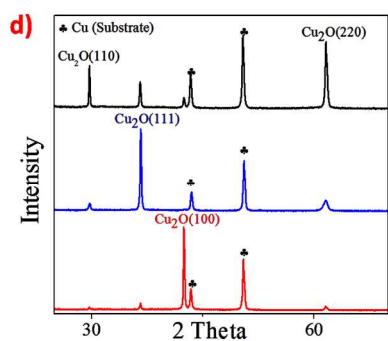
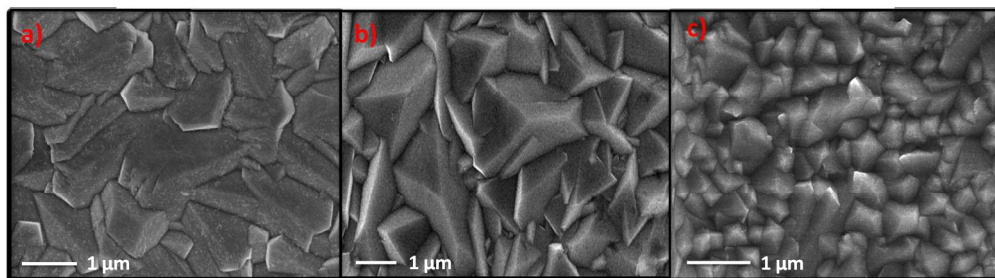
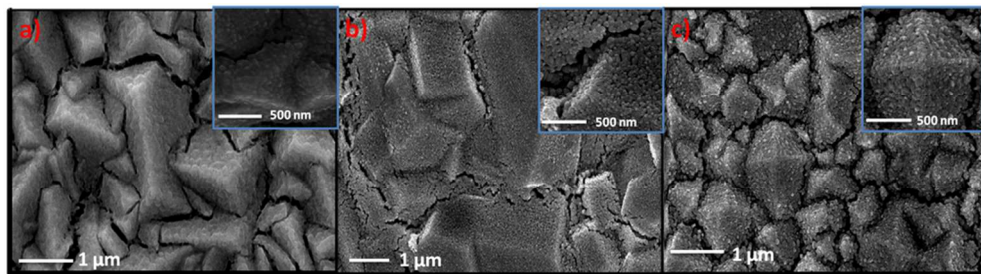


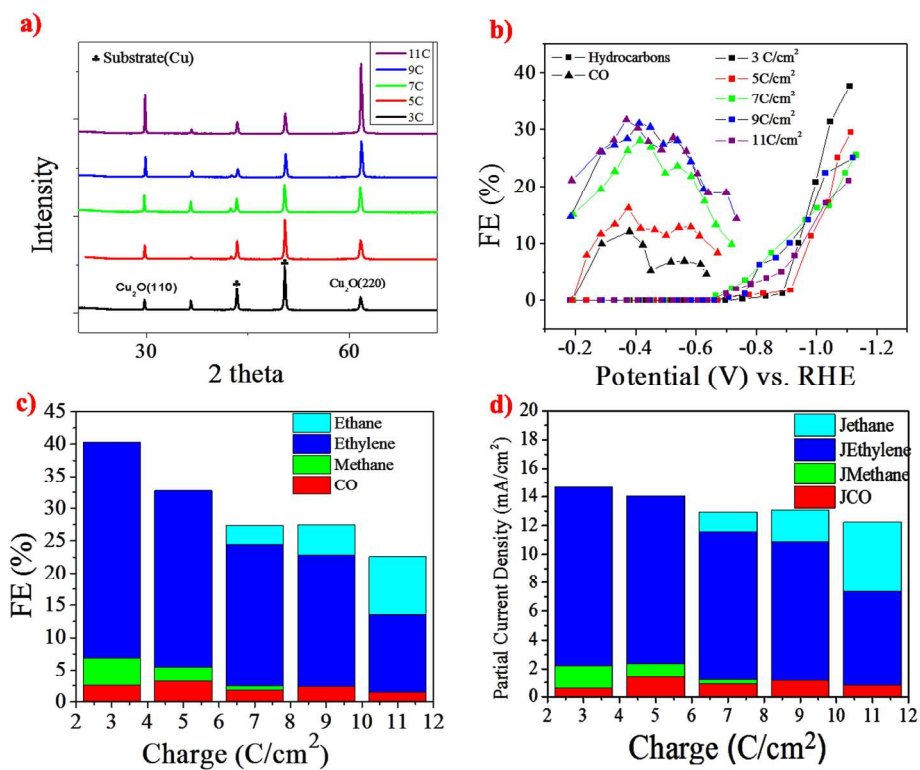
Figure SI7 : Relative FE of the Hydrogen evolution reaction as a function of initial oxide thickness



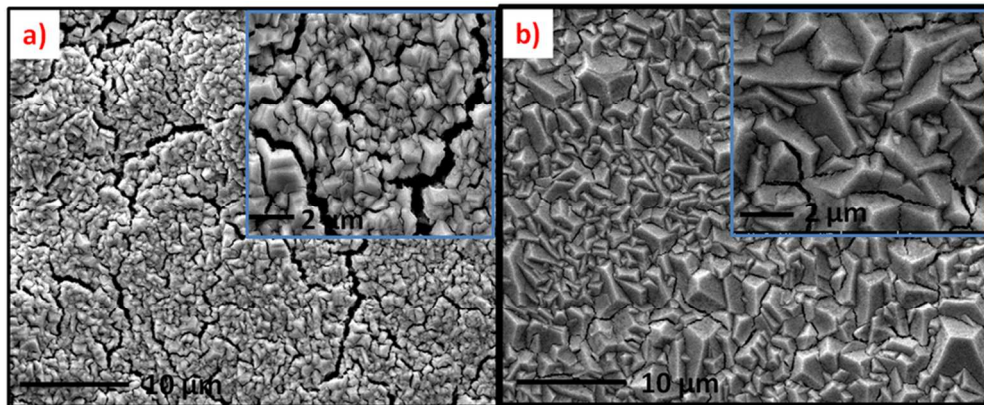
206x138mm (300 x 300 DPI)



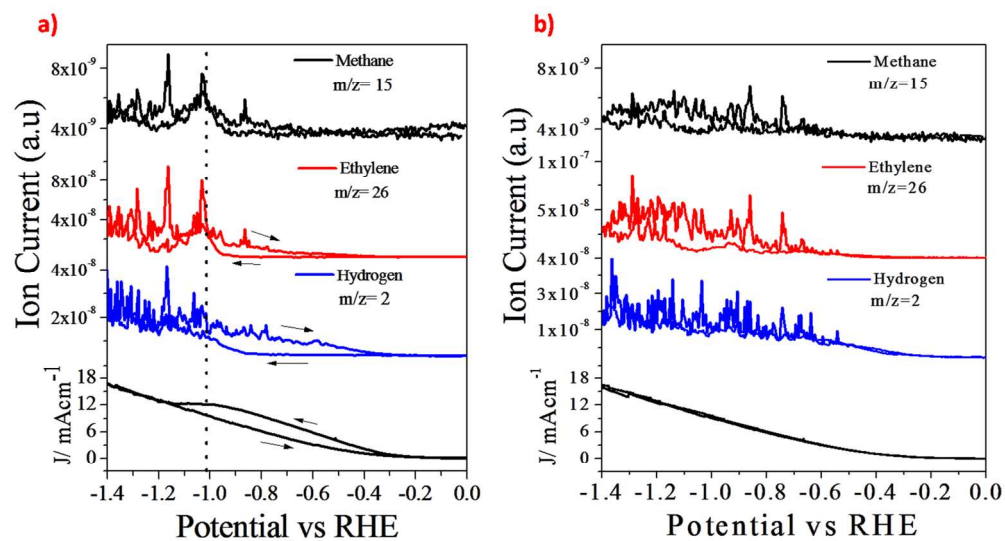
86x24mm (300 x 300 DPI)



188x145mm (300 x 300 DPI)



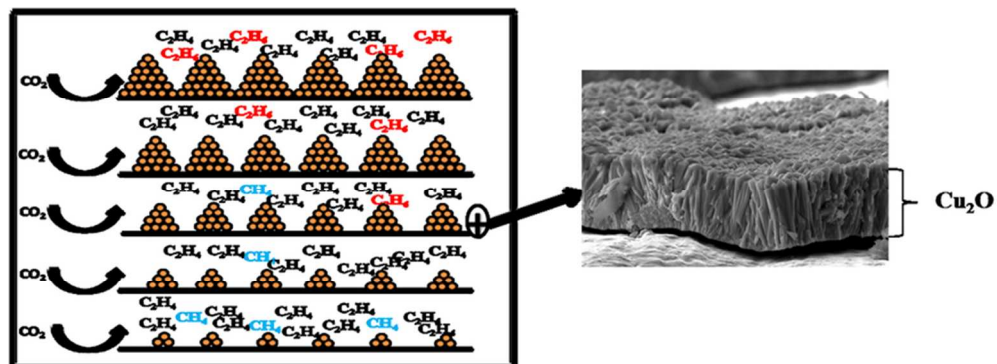
85x35mm (300 x 300 DPI)



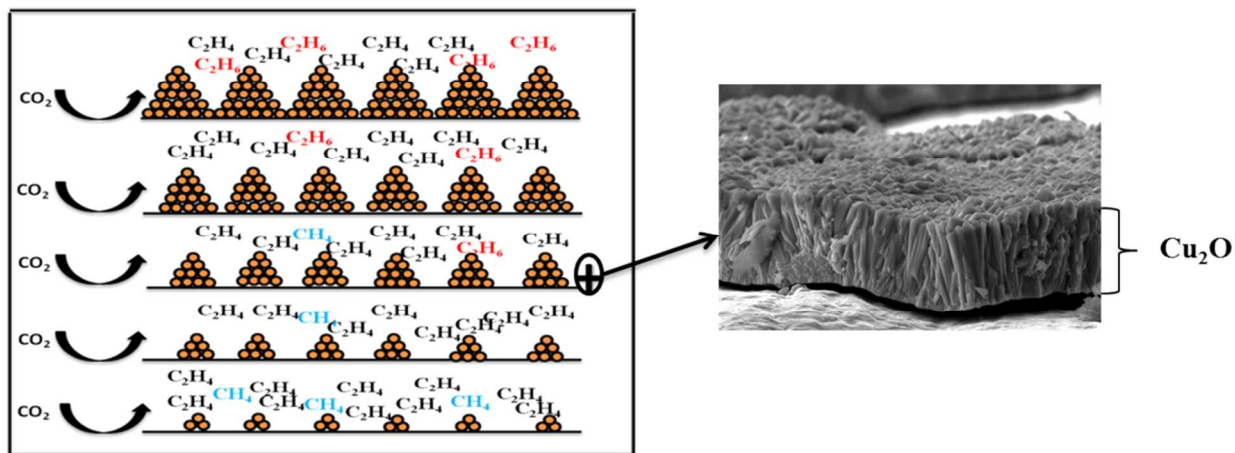
146x83mm (300 x 300 DPI)

Charge passed through	Capacitance	Surface Roughness Factor
3 C/cm ²	1.6 mF	11
7 C/cm ²	5.1 mF	36
11 C/cm ²	9.1 mF	65

83x40mm (300 x 300 DPI)



74x27mm (300 x 300 DPI)



The selectivity difference towards hydrocarbon production during the electrochemical CO_2 reduction on nanoparticulate copper surfaces is presented and discussed.